Crystallization of glass materials into transparent optical ceramics

Iva Milisavljevic, Michael J Pitcher, Jianqiang Li, Sébastien Chenu, Mathieu Allix, Yiquan Wu

Crystallization of glass materials into transparent optical ceramics

Iva Milisavljevic, Michael J. Pitcher, Jianqiang Li, Sébastien Chenu, Mathieu Allix, Yiquan Wu*

I. Milisavljevic, Dr. Y. Wu
Kazuo Inamori School of Engineering, New York State College of Ceramics, Alfred University, Alfred, New York 14802, United States
E-mail: wuy@alfred.edu

Dr. M. J. Pitcher, Dr. M. Allix
French National Centre for Scientific Research (CNRS), CEMHTI UPR3079, University of Orléans, F-45071 Orléans, France

Dr. S. Chenu
Institute of Research for Ceramics (IRCER), UMR CNRS 7315, University of Limoges, F-87068 Limoges, France
Rennes Institute of Chemical Sciences (ISCR), UMR CNRS 6226, University of Rennes, F-35000 Rennes, France

Dr. J. Li
School of Materials Science and Engineering, University of Science and Technology Beijing, Beijing 100083, P. R. China
Institute of Process Engineering, Chinese Academy of Sciences, Beijing 100190, P. R. China

Abstract

Recent advancements in transparent ceramics development have ensured a mainstream research interest in this family of materials, which have been found promising for a broad spectrum of applications. In addition to the widely-used transparent ceramics synthesis approach involving the polycrystalline powder preparation followed by the green body forming and sintering,

crystallization of glass into transparent ceramics has emerged as an alternative but complementary trajectory for obtaining these materials, which circumvents some of the long-standing technical difficulties associated with the traditional fabrication approach. Through the process of full bulk glass crystallization, the method allows for the synthesis of high-density/low-porosity transparent ceramics of stable and metastable phases or even non-cubic structures, which are difficult to obtain using the traditional processing methods, at temperatures far below the typical powder sintering temperatures. This article presents a brief survey of the science regarding the origins of the transparency of ceramics and the principles of light-matter interaction, followed by a detailed overview of the materials systems and techniques used for the preparation of transparent ceramics, which exhibit optical transparency in the visible spectrum, through the glass crystallization route. Finally, the review provides authors' insights into the future trends and research directions of the glass crystallization into transparent ceramics, aimed to encourage a widespread application of this novel concept in the fabrication of next-generation materials.

Keywords: full bulk glass crystallization, microstructure, metastable structure, dense, transparent ceramics, optical materials

1. Transparent ceramics

Interest in transparent ceramics has steadily increased since the first report and the great commercial success of General Electric's Lucalox, fully polycrystalline transparent Al_2O_3 ceramics, developed in the late 1950s. [1] Soon after this discovery, reports on cubic-structured transparent MgF_2, $PbZr_xTi_{1-x}O_3$, $MgAl_2O_4$ ceramics in the 1960s, and Nd:YAG ceramics in 1995 [2] followed. Transparent ceramics, and among them those that show transparency in the visible

part of the spectrum, which will be discussed in this paper, have a number of technical and economic aspects that make them attractive in comparison to other traditional transparent materials such as single-crystals, glasses, and glass-ceramics, a fact that has gained them a significant amount of research attention. Transparent ceramics are polycrystalline materials with structures (from the atomic to the micron scale) that allow for incoming photons to pass through without significant absorption and internal scattering occurring, which reduces the optical transparency of the material. There are a number of potential sources of light scattering in transparent ceramics, with grain boundaries and porosity typically being the most significant. The influence of grain boundary-induced scattering can be minimized, and transparency correspondingly maximized, by producing ceramics with grain sizes at least 5–10 times smaller than the wavelength of incident light. [3] The presence of porosity, corresponding to ceramics that have not been completely densified, is a significant cause of translucency/opacity in ceramic materials. [4] Pores can be found at grain boundaries, triple point junctions, and inside the grains, and are a significant source of transmittance losses, due to the scattering associated with the substantially different refractive index between the interior of the pore and the matrix material. While a certain fraction of residual porosity can often be eliminated by performing additional post-sintering heat treatments, a certain amount of isolated, closed porosity is generally unavoidable, which is detrimental to transparency. Nonetheless, it is of critical importance that porosity be reduced to minimum achievable levels to reduce optical losses and correspondingly increase transparency. [5] Other issues that can increase light scattering include the presence of secondary phases, material segregation at grain boundaries, impurities, surface roughness effects, etc. [3]

Compared to other transparent materials and especially single-crystals, transparent ceramics show many advantages. In most cases, transparent ceramics can be produced with widely-used heat

treatment equipment, which considerably simplifies the production process and makes it more cost-efficient when compared with commercial single-crystal growth techniques (e.g., Czochralski, Bridgman, etc.), which require complicated and expensive equipment and long, energy-intensive heat treatment cycles. Many of the drawbacks associated with single-crystal growth processes, such as very high processing temperatures, difficulty in achieving chemical homogeneity, requiring expensive crucibles, time-intensive nature, and necessity of post-processing machining, etc., can be avoided by using ceramic fabrication routes. The heat treatment temperatures required to produce transparent ceramics are often substantially lower than in conventional single-crystal melt-growth techniques. As a result, energy costs are reduced and challenges associated with maintaining temperature stability at very high temperatures are avoided. [6] Moreover, ceramic fabrication routes can allow dopant ions to be incorporated more homogeneously, and in much higher concentrations as compared to single-crystal growth techniques, an advantage that is particularly useful in optical applications [7]. Additionally, ceramic fabrication routes enable the production of compositions that cannot be attained using conventional single-crystal growth techniques, for reasons such as the incongruent melting of chemical components [8]. Another useful feature of transparent ceramics technology is that it can allow for the near-net-shape manufacturing of ceramic parts (e.g., dome-shaped ceramics, complex-shape 3-D printed ceramics, etc.), which may reduce the number of machining steps. In addition to the obvious technical advantages of transparent ceramic production processes (such as accessibility to a wide variety of chemical compositions, shapes and sizes, high doping concentrations, etc.), which have been summarized by many authors [1, 3], other advantages exist, including economic factors such as scalability, and functional benefits including being able to

produce ceramic specimens with thermal, mechanical, and optical properties similar or superior to those of single-crystals.

Transparent ceramics have been recognized over time as a promising alternative to single-crystal and glass materials, with suitability for various optical and laser applications. Advances in the field of transparent ceramics have directly enabled the development of various solid-state lasers, such as high-power lasers, high-output microchip lasers, ultrashort-pulse lasers, etc. [9] Furthermore, transparent ceramic materials have shown promise for a range of other applications, including waveguide lasers [10], scintillators [11], high-power light-emitting diodes (LEDs) [12], envelopes in lighting products [13], optical lenses [14], magneto-optical materials [15], and armor ceramics [16], among others. Moreover, due to their typically high hardness and fracture toughness and consequently high scratch resistance, as well as the suitability to small-scale productions, availability of different colors, and higher refraction indices that make them more appealing compared to glass gems, transparent ceramics have also been considered for applications as jewelry and in home decoration. [1]

The majority of transparent ceramic materials that have seen extensive investigation to date have been those with cubic structures ($Y_3Al_5O_{12}$, Y_2O_3, CaF_2, SrF_2, $MgAl_2O_4$, etc.). The reason for this lies in the inherent optical isotropy of cubic materials, while polycrystalline ceramics with lower symmetries exhibit optical anisotropy (i. e. birefringence), resulting in the creation of additional light scattering sites at grain boundaries, due to the discontinuity in refractive index between grains with different orientations (although this complicates the already non-trivial task of fabricating a transparent ceramic [4], such materials have been realized in “out-of-equilibrium” birefringent systems such as tetragonal $Sr\mathit{RE}Ga_3O_7$, hexagonal $Sr_{1-x/2}Al_{2-x}Si_xO_4$, orthorhombic $BaAl_4O_7$ and others, which cannot be attained by classic solid-state reaction, and which will be discussed later

in Section 5). One of the most well-studied transparent ceramic systems is the cubic garnet structure, with $Y_3Al_5O_{12}$ (YAG) likely being the most well-studied composition. [15, 17-19] Cubic sesquioxide compositions with the general formula of M_2O_3, such as Y_2O_3 [20], Sc_2O_3 [21], Lu_2O_3 [22], etc., have also been successfully fabricated as high-quality transparent ceramics. Other ceramic systems such as Al_2O_3 [23], MgO [24], $MgAl_2O_4$ [16], ZrO_2 [14], or even Lu_3NbO_7 [25] and Gd_3TaO_7 [26] with cubic defect-fluorite structures, have also been reported. Non-oxide compositions have also been demonstrated, including nitrides (AlN [27] and AlON [28]), fluorides (MgF_2 [29], CaF_2 [30], SrF_2 [31], and BaF_2 [32]), and chalcogenides, such as sulfides (ZnS [33]), selenides (ZnSe [34]), and tellurates ($KNbTeO_6$ [35]). More recently, transparent ceramics have been successfully fabricated from high-entropy oxide [36] and fluoride [37] compositions, which were previously unattainable using conventional single-crystal growth processes. Moreover, even the non-cubic (anisotropic) hexagonal transparent laser ceramics such as Nd:$Ca_{10}(PO_4)_6F_2$ [38, 39] and Yb:$Sr_5(PO_4)_3F$ [40], for potential solid-state laser and optical applications, have been reported. Other transparent ceramics of note include ferroelectric ceramic compositions such as (1-x)$Pb(Mg_{1/3}Nb_{2/3})O_3$–$x$$PbTiO_3$ (PMN–PT) [41, 42] and $(Pb_{1-x}La_x)(Zr_yTi_z)_{1-0.25x}O_3$ (PLZT) [43] that have seen extensive investigation and application in the field of electro-optical devices.

Many different technologies of varying efficacy have been applied to the fabrication of transparent ceramics. The processes generally follow the same general route as conventional ceramic preparation processes, with the basic steps including powder preparation, shaping, and green body compaction (via uniaxial pressing, cold isostatic pressing, etc.) and sintering. Post-sintering treatments are commonly performed (e.g., hot isostatic pressing), along with final grinding and polishing treatments to produce transparency.

Steps in the transparent ceramics processing before the sintering, such as powder processing and green body formation, are perhaps the most delicate since they largely determine the quality of the fabricated ceramics. A number of different powder preparation routes have been applied so far to the preparation of transparent ceramics. The ultimate goal of any of these methods is to produce powder particles that ensure chemical uniformity and are devoid of secondary phases or impurities, have particles that are uniform in size and shape (ideally spherical), which would ensure good powder compaction in the later stages, and do not form large agglomerates that already contain entrapped pores that would be difficult to eliminate later. In terms of particle size, in most cases, sub-micrometer-sized particles are desirable, as they often result in the fabrication of ceramics with high optical transparency. However, particles that are too small may actually produce the opposite effect due to the formation of strong agglomerates. Therefore, as explained by A. Goldstein [1], whether a powder will be suitable for sintering into transparent ceramics or not will largely depend on its particle size and morphology, presence and structure of agglomerates, and the particles' surface chemistry. Solid-state reactions and wet-chemistry methods, including chemical co-precipitation, sol-gel processing, hydrothermal synthesis, flame spray pyrolysis, combustion synthesis, spray drying, freeze drying, and others, are among the most common powder preparation methods for the fabrication of transparent ceramics. Although some powder preparation methods are more common than others, each of them displays advantages and disadvantages in terms of attaining the best possible quality of transparent ceramics.

Besides powder processing, shaping and green body formation are also some of the key steps in transparent ceramics' fabrication. The main goals of these steps are not only to provide the processed powder with desired shape and size but also a significant degree of densification and to break large agglomerates. Similar to the powder processing techniques, there are many forming

techniques with each of them providing certain advantages. Uniaxial pressing is probably the easiest and the cheapest forming technique, along with cold isostatic pressing.

For more information about different powder preparation and powder forming techniques for the transparent ceramics' fabrication, readers are referred to some of many available review articles on these topics. [1, 4, 44]

This review article focuses on the optical transparency of ceramics in the human eye spectral range, that is, in the visible part of the electromagnetic spectrum. Transparent ceramics technologies have enabled the fabrication of ceramics in a wide optical transparency range to date. Whereas most oxide ceramics have shown transparency in the visible range, many non-oxide materials, such as fluorides, and particularly chalcogenides, are transparent in the infrared spectrum (up to 20 μm for telluride ceramics), thus enabling extensive applications in the medical (disease detection), automotive (night vision), military (thermal imaging, night surveillance), and sensor (pollutant detection in water) fields, among others. However, the current literature has provided few data on transparent non-oxide ceramics obtained through the glass crystallization route. The transparent non-oxide ceramics reported to date have been prepared only through the conventional powder processing approach, such as for ZnS [33, 45], ZnSe [34], $CaLa_2S_4$ [46], and others. One reason for this limitation is the lack of flexibility in the glass forming process to enable fabrication of non-oxide transparent ceramics through glass crystallization. Application of SiO_2 tube furnaces and rocking furnaces, for example, does not allow for the fabrication of large glass composition domains. In contrast, several reports have focused on non-oxide transparent glass-ceramics [47] and transparent glass-ceramics with a refractive index gradient based on the gradient of crystallization. [48] Mechanical milling (mechano-chemical synthesis), for example, has aided in the preparation of amorphous precursor chalcogenide powders, which are typically outside the

glassy domain when synthesized via the conventional melt-quenching technique, and are used in the fabrication of transparent glass-ceramics in spark plasma sintering (SPS) furnaces. [49, 50] However, because of the limitations and reasons described above, this review discusses only transparent ceramics obtained through the glass crystallization route that exhibit optical transparency in the visible spectrum.

2. Light-matter interaction and origins of transparency

A discussion of the transparency of ceramic materials must begin with what *transparency* means, what makes transparent ceramics transparent, when a material is considered translucent, what prevents ceramics from being transparent, and how light scattering plays a role. The simplest explanation of what a transparent ceramic material is uses the analogy of a window, which the human eye can see clearly through and provides an undistorted view of a background placed underneath it (this explanation holds true only for the ceramics transparent in the visible part of the electromagnetic spectrum, which is the focus of this review, as emphasized in the previous section). However, this simplistic description of transparent ceramics has a much more complex explanation based on the physics of the light-matter interaction, as briefly explained in this section. For a more in-depth understanding of all phenomena underlying ceramic transparency, readers are referred to specialized textbooks on solid-state physics, optics, and other related subfields of physics. [51-53]

On a macroscopic scale, when light travels through transparent ceramics, it penetrates without any disruption. However, a much deeper understanding of this phenomenon (on the microscopic scale) reveals several physical processes resulting from the interaction of light and material, including refraction, reflection, absorption, transmission, and scattering, which are briefly explained here.

When an incident electromagnetic wave passes through transparent ceramics, it transitions from one medium into another medium with different dielectric properties. Regardless of whether the first medium is vacuum, gas and/or air, or even another solid, the changes in the properties between media cause the light path to bend because of consequent changes in the velocity and polarization state of the propagating light wave. This phenomenon, known as *refraction*, is characterized by a unitless parameter called the refractive index (n), describing the change in the light velocity between the vacuum and another medium (e.g., ceramics). A closely related phenomenon is the *reflection* (R) of light, which is defined by the refractive indices of the two media (n_1 and n_2). Near the normal incidence of light onto a fully flat and smooth surface [1], reflection represents the primary reflectance from the material, also known as the Fresnel reflectance, defined as:

$$R = \frac{(n_1 - n_2)^2}{(n_1 + n_2)^2} \quad (1)$$

Ceramic materials with high refractive indices also show high reflectance R; thus, less incident light is transmitted through the material, and the material's properties and applications are consequently affected. More generally, for incident media other than a vacuum, the refractive index can be represented with a dimensionless parameter $n = n_1/n_2$. The above equation can be expressed in the following more common form:

$$R = \frac{(n-1)^2}{(n+1)^2} \quad (2)$$

The light shone on a transparent material inevitably loses a portion of its incident energy before exiting the material as transmitted light, owing to the processes of reflection, absorption, and scattering. The ratio among the intensities of these processes depends on the physical characteristics of the solid and the presence of impurities. To limit the "surface effect" to Fresnel reflection only and avoid any backscattering of the incident light from surface irregularities, optical polishing of the ceramics' surface is necessary, because smoother, flatter surfaces are less likely

to scatter the incident radiation beam. However, a portion of the incident light passing through the material bulk is also absorbed and scattered by the material on its optical path by the time the light reaches the other side of the polished ceramic, thus attenuating the intensity of the transmitted light. The intensity of the traversing light exiting the ceramics can be expressed with the Lambert-Beer equation:

$$I(t) = I(0)\exp(-\alpha \cdot t) \quad (3)$$

where t is the thickness of the ceramic sample, i. e., the distance that the light travels through the ceramics. $I(0)$ and $I(t)$ are the intensities of the incident and light at the exit from the ceramics, respectively, and α is the attenuation coefficient. In a homogeneous medium, the light attenuation is due to absorption by the material. However, the choice of an appropriate material composition can minimize or even avoid absorption. In contrast, in a heterogeneous environment, impurities in the material cause the light to scatter in directions different from the initial direction of travel, thereby attenuating the intensity of the transmitted light.

Transmittance is a parameter quantifying the amount of incident light transmitted through a sample. In a very general sense, the transmitted light (T) is the amount of incident light shone on the polished ceramic plate that remains after loss (attenuation) due to reflection (R), absorption (A), and scattering (S), as mathematically presented below:

$$\mathrm{T} = 1 - \mathrm{R} - \mathrm{A} - \mathrm{S} \quad (4)$$

More precisely, the transmittance represents the ratio between the transmitted (I) and incident (I_0) light, multiplied by the theoretical transmittance (T_{th}), which is the maximum transmittance that a material can achieve ($T_{th} \equiv T_{max}$) on the basis of its optical properties and an average of the refractive indices of all phases in the material and surrounding medium [54], as presented in the following expression:

$$T = T_{th}\frac{I}{I_0} \quad (5)$$

If no scattering or absorption occurs in the material after the incidence of a coherent light beam onto the surface of a perfectly optically polished ceramic plate in vacuum or air, then, if the attenuation coefficient is assumed to be zero ($\alpha = 0$), the theoretical (maximum) transmittance T_{th} can be obtained as follows:

$$T_{th} = \frac{2n}{n^2+1} \quad (6)$$

The schematic presented in **Figure 1** below depicts the optical path of light traversing a transparent ceramic material, summarizing all processes occurring along the way.

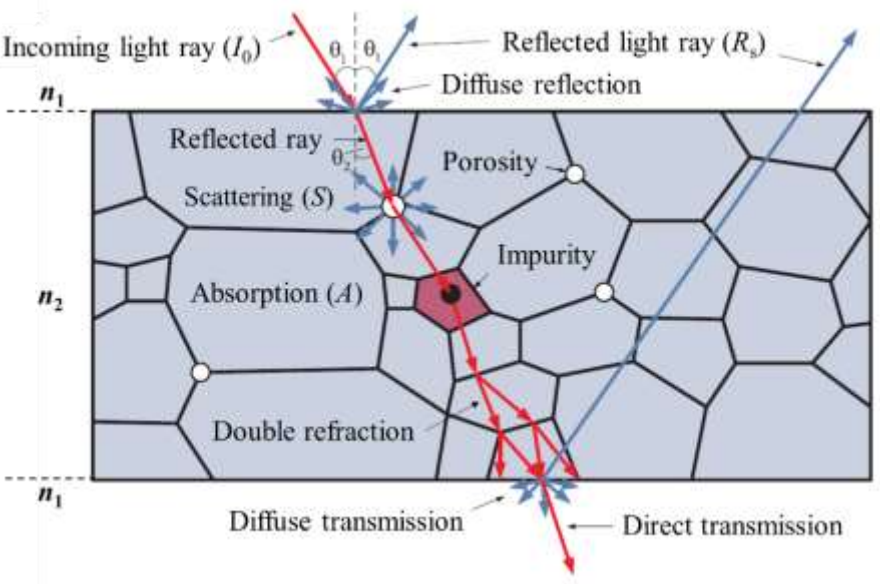

Figure 1. Schematic illustrating an optical path of light traversing transparent ceramics. [55]

One of the most reliable ways to quantify the transparency of a ceramic is measuring the in-line transmittance. This analysis includes the measurement of transmittance T with a UV-vis spectrometer, by shining light from the source at a 90° angle (or as close to a normal angle as possible) onto the surface of a polished ceramic and detecting the transmitted light with a detector positioned at a detection angle 0.5° or smaller. [54] This measurement provides results represented

as a percentage of the maximum possible transmittance, which, according to the above formula, can never reach 100%, even in a perfect, impurity-free homogeneous material.

A major challenge in transparent ceramics technology has been the decrease in transparency loss caused by scattering. Most light-scattering sources arise from the ceramics' microstructure, such as its pores, grain boundaries, grain size, and structure, as well as the presence of impurities, secondary phases, and birefringence effects. These scattering centers may act as small dispersion zones of different refractive indices [1] which cause the incident light to diverge from its initial optical path, thereby decreasing the amount of the transmitted light (**Figure 2**). However, scattering should not be treated as a simple dispersion of light when it meets a barrier on its path. After reaching the zone with different optical properties, the incident electromagnetic wave interacts with the electric and magnetic dipoles and multipoles of the scattering center, thus causing the traversing light to scatter (radiate diffusively). The basis for this phenomenon is Mie scattering theory, which provides a generalized analytical solution to electromagnetic wave scattering by a homogeneous metal sphere of a size identical to or larger size than the wavelength of the traversing light, with a refractive index different from that of the medium through which it is passing. However, because the Mie scattering model is complex or may have limitations, other simpler models are more frequently used to describe the scattering phenomenon, such as the Apetz-van-Bruggen model. [56]

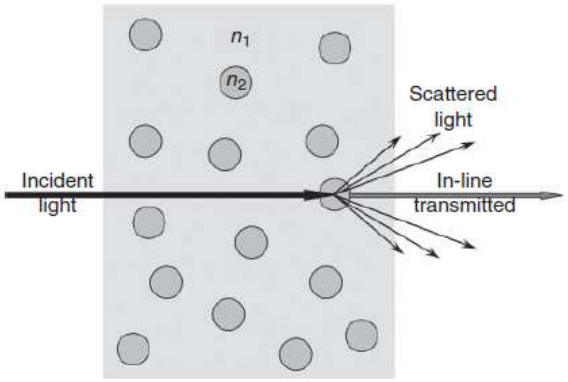

Figure 2. Schematic illustration showing the in-line transmittance measurement of ceramics with refractive index n_1, exhibiting scattering from the light-scattering centers with an n_2 index of refraction. [1]

Porosity is a major contributor to the transmittance loss in transparent ceramics. Trapped pores, whether they are intergranular or intragranular, are gas-filled voids inside ceramics. When the light traversing through a ceramic encounters a pore, a significant diffraction index difference between the ceramic matrix and gas media causes the light to reflect and refract from the pore's surface, thus resulting in transmittance loss. Therefore, residual porosity must be avoided during transparent ceramic processing, because even 0.1% porosity with a size <100 nm is deleterious to in-line transmittance. [56] As the pore size decreases, the pores' contribution to light scattering becomes less pronounced.

Grains and grain boundaries are another source of transparent ceramic transmittance loss. The chemical composition and structure [57] of grain boundaries often differ from those of the bulk grains, thus resulting in significantly different optical properties between species. This difference may cause the grain boundaries to act as scattering centers for light. Trapped pores, as well as impurities and secondary phases, can be found at grain boundaries. Although all these inclusions act as major scattering centers, grain boundaries alone rarely pose issues in terms of transparency, because of their small thickness, on the order of nanometers. [1]

Secondary phases and impurities originating from the raw material, unreacted (undissolved) chemical species, or sintering additives, which typically have chemical and physical properties different from those of the matrix material, are the major light scattering centers in ceramics. Therefore, the raw materials and fabrication approaches must be carefully chosen to decrease the contamination at each step of transparent ceramic processing. The same holds true for choosing and determining the optimal amount of sintering aids to facilitate transparent ceramic sintering but to avoid the formation of scattering centers in the form of secondary phases, usually at the grain boundaries (e.g., undissolved sintering aids or amorphous phases). [44]

Finally, the material's crystal structure is another crucial parameter substantially affecting ceramic transparency. Ceramics with a cubic crystal structure comprise grains that all exhibit optical isotropy, thus ensuring high optical homogeneity in these materials. Consequently, when light passes through cubic ceramics, it is not scattered by the grains, because they all have identical optical axes and thus exhibit the same optical properties. In contrast, ceramics with low symmetry (non-cubic) crystal structures exhibit high optical anisotropy, that is, *birefringence*. In birefringent ceramics, different light polarizations exhibit different refractive indices, thus endowing each light polarization component with three distinct refractive indices along the *x*-, *y*-, and *z*-axes (n_x, n_y, and n_z). [1] The optical properties of adjacent grains in ceramics with non-cubic crystal structures may exhibit different optical properties, which cause the light to scatter as it travels across the grain boundaries. Nevertheless, although most research in the transparent ceramics field has been performed on ceramics with a cubic crystal structure (e.g., $Y_3Al_5O_{12}$, Y_2O_3, $MgAl_2O_4$, MgO, CaF_2, SrF_2, and other), recent advances in this field have enabled the fabrication of ceramics with non-cubic symmetries, such as Al_2O_3 [58], Nd:$Ca_{10}(PO_4)_6F_2$ [39], hydroxyapatite ($Ca_{10}(PO_4)_6(OH)_2$) [59], and others. Substantial progress in this area has been enabled by novel ceramic processing

technologies, which have allowed for the fabrication of ceramics with nanosized grains [39, 59] or with highly oriented grains under a strong magnetic field. [60] These and many other approaches have helped alleviate the deleterious birefringence effects in non-cubic transparent ceramics. Mie scattering at grain boundaries, due to birefringence from the grains with different crystal orientations, can strongly be inhibited by decreasing the average grain size in ceramics to a range comparable to the wavelength of the incident light (also known as Rayleigh scattering), as illustrated in **Figure 3**.

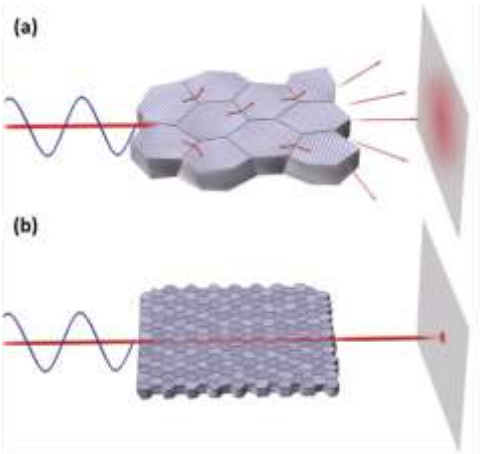

Figure 3. Schematic of the grain size effect on Mie scattering in non-cubic ceramics with grains (a) larger than and (b) comparable to or smaller (Rayleigh scattering) than the wavelength of incident light, and consequent effects on the amount of transmitted light. [39]

However, despite the high in-line transmittance, an increase in the sample thickness of birefringent ceramics may still severely decrease optical transmission, because of the light scattering from grain boundaries. Therefore, for this group of ceramics, in-line transmittance should be obtained with the following approximation from Apetz and van Bruggen, which has roots in Rayleigh-Gans-Debye theory [56]:

$$T = (1 - R_s) \exp\left[-\frac{3\pi^2 r \Delta n^2 t}{\lambda_0^2}\right] \quad (7)$$

by considering sample's thickness (t), the wavelength of incident light (λ), grain size (r), and refractive index difference (Δn) that corresponds to the birefringence averaged over all grain orientations in the sample. R_s is the loss due to the reflectance from the two sample's surfaces (incident and exiting surfaces for the light beam) at the normal angle of incidence.

In general, this parameter is unaffected by the sample's thickness only when a sample exhibits maximum (theoretical) transparency; however, maximum transparency is very difficult to achieve, in practice. In contrast, if the transparency is below the maximum value, scattering prevails, and transmittance is likely to continue to decrease with increasing material thickness. This problem is particularly apparent in applications in which the materials are expected to have high thickness (such as ceramic fiber, as an extreme example). In general, materials with an in-line transmittance 65% or greater are considered transparent in samples with a minimum of 2 mm thickness. In contrast, ceramics with in-line transmittance in the 15–65% range are considered translucent. [1] Below 15% transmittance, ceramics are considered opaque. Another critical detail is that the qualitative evaluation of a ceramic's transparency, by placing a ceramic piece flat against a printed background, is not a sufficiently reliable method of assessing transparency. Instead, the samples should be placed at least 2 cm above the background, and the image should be observed through the material. This method is considered the standard or suggested method of transparency evaluation, and it helps efficiently discriminate between transparent and translucent ceramics, because the latter are strongly affected by light scattering, which blurs the image observed through the sample [1, 61, 62]. Finally, qualitative results should be supported by quantitative data obtained from in-line transmittance measurements. Nevertheless, although placing ceramics in immediate contact with the background provides insufficient evidence of transparency, most of the available literature on transparent ceramics, including the references cited in this review, have used this

method for evaluation of optical transparency. Therefore, all materials discussed herein that exhibit transparency in the visible range when in contact with the background are considered transparent. Finally, perfect transparency is not always mandatory; in general, the required transparency level depends on the application of the transparent ceramics. For example, laser applications require extremely high transparency, whereas the media need not be perfectly transparent for solid-state lighting. Moreover, in the latter case, light scattering centers may even be beneficial for light extraction by making the lighting more homogeneous.

3. Sintering techniques for transparent ceramics

Many sintering approaches have been successfully applied in the fabrication of transparent ceramics over many years. In the light of the discussion in the previous section, the main goal of any technique used for transparent ceramics sintering is to decrease the light scattering associated with the transmittance loss from the most common scattering centers, primarily pores and grain boundaries.

Pressureless vacuum sintering has become the method of choice for fabricating various oxide transparent ceramics, especially garnets [19, 62, 63] and sesquioxides [21, 64]. Vacuum sintering involves conducting a high-temperature heat treatment in a vacuum environment, which assists the densification process. Vacuum sintering is often followed by an annealing treatment at lower temperature in air, which serves to eliminate oxygen vacancies and other structural defects induced by the reducing effect of vacuum, eliminating dark coloration, and correspondingly increasing transparency. Other controlled atmospheres such as oxygen or hydrogen are also used, depending on the requirements of the specific material system. [11, 65] Vacuum sintering has been found to

aid in fabrication of many high-density (low-porosity) transparent ceramics. Nd^{3+}-doped YAG is among the most researched and most successfully fabricated transparent ceramics through this technique. The porosity of this material can reach less than 0.2%; however, the high-temperature processing, aided by the presence of sintering additives added to the material to facilitate densification through the formation of a liquid phase, enhances the grain boundary diffusion, thus resulting in substantial grain growth (micrometer range). A typical example of the polished surface of YAG transparent ceramics obtained via vacuum sintering is presented in the scanning electron microscopy (SEM) micrograph in **Figure 4(a)**. Although visually very transparent, these ceramics may exhibit substantial light scattering from large grains and grain boundaries, in addition to residual porosity. Therefore, ceramics consolidated by pressureless sintering are frequently subjected to a post-sintering hot isostatic pressing (HIP) treatment in gases that exhibit low solubility in the processed ceramics, which serves to reduce the residual porosity of the final ceramic product, and correspondingly increase optical transmittance. [66-68] Tsukuma et al. [69] have proposed the microstructural evolution model for pore elimination, which was developed on the basis of the HIP processing of transparent 8 mol.% Y_2O_3–ZrO_2 (YSZ) ceramics, and has been found to aid in the fabrication of many transparent ceramic oxides. The model suggests that if pre-sintering is conducted at lower temperatures, the created pores are more likely to be removed from the material during the HIP process and consequently enhance the material's transmittance. In contrast, high-temperature pre-sintering creates pores, which tend to become closed intergranular pores with the growth of the surrounding grains and are difficult to eliminate from the system by using the isostatic pressure of the HIP process.

Despite the fact that simple uniaxial and cold isostatic pressing are likely the most common methods for ceramic green body forming, a number of alternative approaches to green body

preparation and shaping have been reported. These methods include but are not limited to various casting methods such as gel-casting [70], slip-casting [71], and tape-casting [72]. More recently, 3-dimensional (3-D) printing techniques have gained popularity for the preparation of green bodies from powder slurries. [73]

In addition to vacuum sintering, hot-pressing is another sintering method that commonly sees application for transparent ceramics. The combination of moderate pressure and high temperature during sintering produces better contact between particles in the powder compact through particle rearrangement, thereby enhancing densification with respect to the coarsening process, particularly in the final stages of sintering. The material transport occurring during the pressure-assisted sintering, mainly grain boundary and volume diffusion, is greatly aided by the plastic deformation and creep mechanisms. [74] Simultaneous action of these processes contributes to very rapid densification rates, thus resulting in a grain growth inhibition effect and enabling the fabrication of fine-grained ceramics with many superior properties, including high mechanical strength. Most importantly, as briefly explained in the previous section, the grain growth suppression resulting from external pressure application is an important mechanism for achieving high optical transparency, particularly in non-cubic (birefringent) ceramics. Hot-press sintering is generally conducted at moderate loading pressures (< 100 MPa) and relatively high temperatures; however, enhancing the densification rate enables sintering at markedly lower temperatures and shorter sintering times than those in pressureless sintering. Moreover, the applied pressure aids in decreasing the porosity, particularly closed porosity, probably because of enhanced mass transport. [1] The effectiveness of external pressure on the densification rate is defined by the size and inter-connectivity of powder particles and the presence of liquid phases from sintering aids (e.g., LiF in $MgAl_2O_4$ [75]), which stimulate viscous flow under the employed sintering conditions. A HIP

process often follows a hot-pressing process to eliminate residual porosity and increase the transparent ceramics' transmittance. Hot-pressing has been demonstrated to be effective for producing a variety of transparent ceramic compositions, including fluorides [30, 76], $MgAl_2O_4$ spinel [77, 78], Y_2O_3 [79], ZnS [33], and even $(K_{0.5}Na_{0.5})NbO_3$ (KNN) [80]. Additionally, a novel hot-pressing method that is conducted at ultra-high pressures (up to 15 GPa) has been successfully used to produce transparent ceramics with very small grain sizes. The application of ultra-high pressure allows for densification to be achieved at very low temperatures (~500^{o}C and lower), which inhibits grain growth and enables the fabrication of nanoceramics with very high optical transparency. Consequently, the material's mechanical properties are improved, and the fabrication of transparent anisotropic structures is enabled, owing to the negligible birefringence effect of nanoceramics. However, a drawback of this technology is that it is restricted to the fabrication of samples with very small sizes, because of equipment limitations. Nevertheless, highly transparent YAG nanoceramics have been obtained using this sintering technique, at pressures as high as 2–5 GPa and temperatures as low as 300–500^{o}C. [81] Moreover, the sizes of the remaining pores become so small after sintering at such high pressures that, even if their number density is high, they do not significantly contribute to optical scattering and therefore reduce optical transmittance, because their size is in the nanometer range—much smaller than the wavelength of incident light. As explained by Zhang et al. [78], the transparency mechanism of ceramic samples obtained under GPa pressures does not entirely follow the rules of the traditional transparent ceramic processing. Therefore, to achieve high transparency, the size of the pores (D) must meet the criterion $\chi = \pi D/\lambda$ for the given wavelength of the incident light (λ), for which $\chi < 1$. Another important sintering technique that has widely been used for the fabrication of transparent ceramics is Field-Assisted Sintering Technique (FAST), also known as Spark Plasma Sintering

(SPS). SPS is a relatively new technique that allows for sintering to be conducted at lower temperatures and with significantly reduced ramping and dwelling times as compared to other sintering techniques. Although SPS is most commonly conducted with graphite dies that limit applied pressure to ~100 MPa, it is also possible to use metal alloy tooling that allows for pressures up to several hundreds of MPa to be applied, which assists particle packing and the powder densification. SPS is fundamentally different than other sintering techniques, where conventional heat treatment processes heat a specimen indirectly through radiation, conduction, and convection from heating elements in the furnace chamber: in SPS, specimen heating is achieved by passing a high-density electric current directly through the sample and die in which it is contained, with temperature being increased via Joule heating. [4] Densification is achieved at a substantially higher rate than in other sintering processes and pressure-assisted sintering, such as hot-pressing and HIP [4], which minimizes the time over which grain growth can occur. Because of the ability to achieve densification without substantial grain growth, SPS enables the consolidation of ceramics with nanoscale grains, decreasing scattering from grain boundaries and improving optical transparency, particularly for non-cubic ceramics. However, for some materials, such as $MgAl_2O_4$ spinels [82], lower heating rates (below the usual rates in SPS) do not significantly influence grain growth; instead, they substantially influence the decrease in porosity to below 0.5%, thus increasing the transparency and mechanical strength of the material. Similarly to hot-press sintering, the application of external pressure during SPS helps achieve nanometer-sized porosity, as in the case of Cr^{3+}-doped $ZnGa_2O_4$ [83], in which the main source of optical loss is the pores at the grain boundaries and triple junctions (~50 nm diameter). The SPS processing of this material has enabled the fabrication of transparent ceramic pieces (~78% in-line transmittance at 2.5 μm—a value close to the results obtained for the single-crystal of the same composition), because of the

limited number of scattering centers associated with very low porosity, very thin grain boundaries, and average grain size of approximately 600 nm, as shown in the electron backscatter diffraction (EBSD) and transmission electron microscopy (TEM) images in **Figure 4(b)–(d)**. The addition of sintering additives during SPS sintering, as in other sintering techniques, facilitates densification and the alleviation of the deleterious effects of the light scattering from pores. However, sintering aids should be used with caution because they also promote grain growth and, therefore, facilitate the creation of new scattering centers. SPS has been reported to be a very effective method to achieve densification in a number of transparent ceramic material systems with very small crystallite sizes and with cubic and even non-cubic symmetries, such as $MgAl_2O_4$, $ZnAl_2O_4$, $ZnGa_2O_4$ spinels [83-85], Sc_2O_3, Y_2O_3 and Lu_2O_3 sesquioxides [86], YAG [87, 88], α-Al_2O_3 [89], 8 mol. % Y_2O_3–ZrO_2 (YSZ) [90], MgO [91], CaF_2 [92], $Sr_5(PO_4)F$ [40], ZnS [93], AlN [27], etc. A common problem associated with SPS sintering is carbon contamination of the ceramics from graphite tools. Post-annealing in the air or other gas environments in pressureless conditions often follows SPS processing, which helps remove a portion of the carbon diffused into the ceramics. However, this post-processing can also lead to pore swelling, owing to the reaction of carbon with oxygen (creation of high-pressure CO_2 and CO gases), which can sometimes affect material transparency. Importantly, the dark coloration of ceramics after SPS processing is not necessarily associated with carbon contamination. The dark color may arise from processing in a reducing atmosphere, which creates defects (e.g., oxygen defects) responsible for the dark appearance (the same effect is observed in ceramics processed in a vacuum furnace). Annealing in the air or other oxygen-rich environments is also beneficial for eliminating coloration.

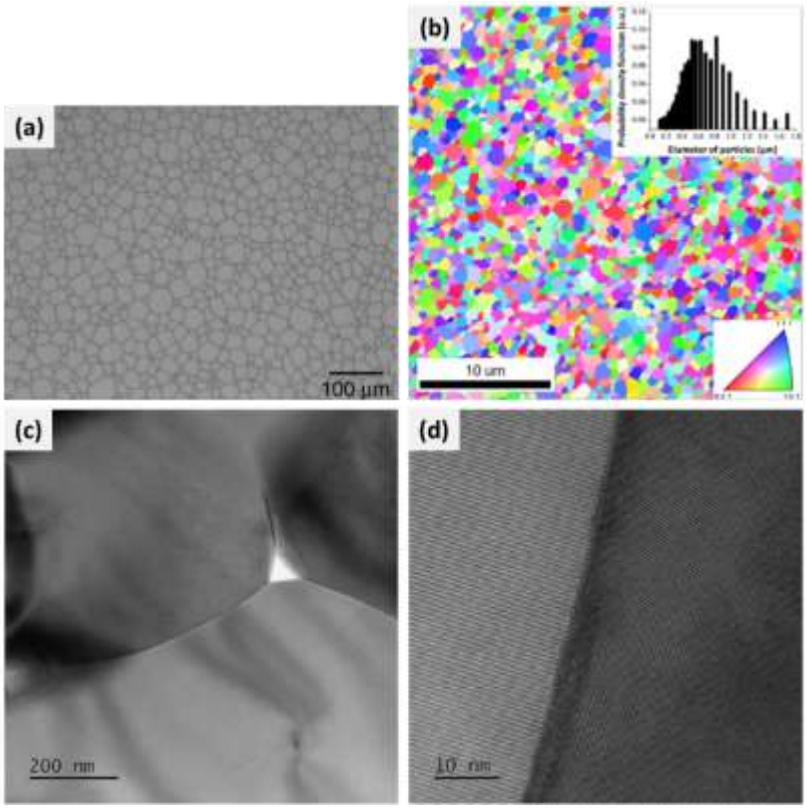

Figure 4. (a) SEM micrograph of YAG transparent ceramics fabricated via pressureless vacuum sintering at 1800°C for 16 h; [62] (b) EBSD map of $ZnGa_2O_4$ transparent ceramics with grain size distribution chart in the inset; (c) TEM micrograph showing porosity at the grain triple junction, and (d) high-resolution TEM image of the thin grain boundary in Cr^{3+}-doped $ZnGa_2O_4$ transparent ceramics. [83]

Microwave sintering is yet another sintering technique worthy of mention in the context of transparent ceramics, which has seen increasing interest in recent years. However, compared to other techniques, such as SPS or vacuum sintering, which have been widely used in both academic research and industry for the fabrication of high-quality transparent ceramics of a variety of materials systems, microwave sintering is still at a relatively early stage of development. Densification of transparent ceramic systems by microwave heating has been successfully conducted in compositions such as YSZ [94] and $MgAl_2O_4$ [95]. Microwave sintering enables the densification of ceramics through the absorption of microwave radiation by the material and conversion of the electromagnetic energy to thermal energy, which is then distributed with high

uniformity throughout the sample. However, the degree of microwave absorption is highly material-dependent and is considered to be a function of various parameters, including dielectric loss, magnetic properties, electrical conductivity, porosity, and others. Therefore, the materials such as Al_2O_3, ZrO_2, $MgAl_2O_4$, etc., that exhibit either extremely weak or no interaction with the microwave field cannot be heated. In these cases, special inducers such as SiC or charcoal, which are strong microwave absorbers, have to be brought into close contact with the target materials to transfer heat by thermal radiation and allow them to be sintered. In general, the presence of microwave radiation decreases the activation energy of sintering and increases the kinetic energy and diffusion coefficients of the materials, allowing for faster heating rates and lower sintering temperatures compared to conventional sintering techniques. This makes the technique an efficient and cost-efficient alternative for consolidating transparent ceramic specimens. Microwave sintering also allows for much higher grain growth rates; however, the underlying reasons remain incompletely understood. Although the average grain size in $MgAl_2O_4$ is in the submicrometer range, approximately 550 nm [95], thus conferring notable hardness and fracture toughness, this result has been achieved after just 10 min of sintering. Interestingly, with longer sintering times, the remaining porosity increases because of grain sliding, which acts as the primary source of light scattering and decreased optical transmittance in the visible range. The microstructural development of microwave-sintered ceramics is similar to that in conventionally sintered materials, exhibiting normal grain growth; however, some studies have shown that microwave sintering enables almost 20% lower activation energy for grain growth than the conventional heating approach. [96]

Despite the nearly three decades of research and development that have focused on developing high transparency ceramic materials, it is necessary to recognize that many aspects of producing

such materials remain challenging. In most instances, single-crystalline materials still exhibit superior properties relative to analogous polycrystalline specimens, due to the absence of grain boundaries and porosity. Fortunately, however, advances in ceramic technology continue to reduce the gap between the performances of polycrystalline and single-crystalline ceramic materials. [2, 6, 17] Even though both are ceramic materials, for simplicity, polycrystalline materials will be referred to throughout the text as ceramics, whereas for the single crystalline materials, the term single crystals will be used.

It is generally accepted that in order for transparent ceramics to see widespread application, a number of technical challenges related to their fabrication must be either resolved or circumvented using alternative approaches. Most of the currently accepted solid-state technologies can be regarded as costly, as they frequently involve extended high temperature heat treatment cycles, and in certain cases, additional post-sintering heat treatments (e.g., HIP). Furthermore, significant challenges exist with regards to eliminating residual porosity, and either eliminating or reducing the deleterious effects of grain boundaries and secondary phases. Attempting to expand the scope of transparent ceramics to non-cubic systems offers additional complexities.

The present summary overviews literature reports concerning an alternative, but complementary approach to the fabrication of transparent ceramics through crystallization of an amorphous body to form a corresponding polycrystal. The method has been demonstrated to be promising for producing ceramics [97] and high-quality transparent ceramics [98-101] of various chemical compositions, with the advantage that it allows for some of the previously discussed challenges associated with conventional sintering routes to be circumvented. Through the process of full glass crystallization, linked to the low-temperature synthesis and the chemical and structural homogeneity of glass (which provides relatively low kinetic energy barriers to reaction and

sintering), new metastable crystalline phases can be accessed that are difficult, if not impossible, to obtain via the conventional solid-state reaction approaches. The paper will conclude with a summary and a future outlook, including an overview of some of the challenges associated with this particular transparent ceramic fabrication approach.

4. Fabrication of transparent ceramics by crystallization from glass

Glasses are a class of materials that lack long range order, and generally exhibit high chemical homogeneity, high relative density, and low porosity. The controlled partial crystallization of a glass results in the formation of a glass-ceramic composite, comprised of randomly distributed crystallites and residual glass phase. [102] Depending on the size and the amount of the formed crystallites and the difference between the refractive indices of the ceramic and residual glass phases, glass-ceramics can be made transparent and with properties suitable for optical applications. [103-105] However, the fabrication of glass-ceramics with acceptable optical properties is a challenging task, as the resulting optical transmittance is generally determined by the number density of crystallites that are produced, which is difficult to control. Typically, the optical transmittance of the glass-ceramic materials is achieved through the controlled formation of low to moderate volume concentrations of nanoscale crystallites with sizes much smaller than the wavelength of the passing visible light, although it has been proved that even a high volume fraction of micrometer-sized crystallites may result in the fabrication of highly transparent glass-ceramic samples. [106] A general strategy for the fabrication of transparent glass-ceramics follows careful precipitation of crystallites from the glass matrix, with sizes smaller than 15 nm, and the

refractive index difference (Δn) of not more than 0.1 (although these values should not be considered as strict cutoffs). [107]

However, the fabrication of transparent crystalline materials such as glass-ceramics using glass-forming processes is not a new idea. In 1969, Beall and Duke [108] discussed the advantages of glass-ceramic materials over transparent glass or ceramics (e.g., thermal stability, low thermal expansion, high strength, etc.), formed by conventional ceramic processing methods, and emphasized the range of their applicability accessible by using a variety of glass-forming techniques. In their work, the authors investigated the formation of transparent glass-ceramics within the β-quartz solid solutions, such as the SiO_2–$LiAlO_2$–$MgAlO_4$–$ZnAl_2O_4$ system in the presence of ZrO_2 and/or TiO_2 added to instigate phase separation, nucleation, and crystallization during the annealing step. As a result, they identified three glass-ceramic compositional areas with unique physical properties, which all exhibited high optical transparencies; these transparent β-quartz solid solution glass-ceramics were classified as ultra-low expansion materials, refractory and colorless materials, and high electrical resistivity-low dielectric loss materials. Highly transparent glass-ceramics can also be achieved in spinel systems (aluminates, gallates, ferrites, etc.) with AB_2O_4 unit cell formula and mullites (binary SiO_2–Al_2O_3 system), as demonstrated by the same authors. [108, 109] These transparent glass-ceramic systems' success and broad applicability lie in the precipitation and slow growth of nanocrystallites dispersed throughout the parent glass phases that provide functionalities to these materials. [107] If the formed nanocrystallites are smaller than the incident light or have refractive indices similar to the parent glass phase, it is expected that glass-ceramics will exhibit high transparency and will be suitable for the applications in optics and photonics. [109] However, exceptions to these rules exist, such as in the case of the micrometer-sized crystallites reported by Berthier et al. [106] The

functionalization of transparent glass-ceramics was further extended by doping with rare-earth ions, which introduced luminescence characteristics to this group of materials that displayed a notably different nature than those of their glass counterparts. [110] The rare-earth doping opened up a new alley of potential applications, such as in optical amplifiers, solar collectors, laser applications, and many other photonic devices [109], combining the optical advantages of transparent glass-ceramics with the simplicity of the glass-forming processes.

Another significant milestone in the history of transparent glass-ceramic materials was the observation of oriented surface crystallization from glass that supported coherent light propagation. Such a feature of transparent glass-ceramics is also responsible for the effects of second-order optical non-linearity [111], the localized second harmonic generation when irradiated with a focused laser, and others. In terms of achieving high transparency, bulk homogeneous nucleation and crystallization in these glass-ceramics must be avoided since the randomly oriented crystallites act as scattering centers of the penetrating light. In their 2001 study, Fujimoto et al. [112] fabricated for the very first time transparent $BaO–Ln_2O_3–TeO_2$ (Ln = La, Pr, Sm, Eu, and Er) tellurite glass-ceramics; however, the authors also observed that the crystallization mechanism largely depended on the ionic radius of the Ln dopant used in the glass system. Oriented surface crystallization was observed in the glass-ceramics with La^{3+} and Pr^{3+} species, whereas Sm^{3+}, Eu^{3+}, and Er^{3+} facilitated bulk crystallization. In a later study by Yamazaki et al. [111], the authors obtained transparent glass-ceramics through the surface crystallization in $35BaO–15TiO_2–50GeO_2$, $28BaO–18TiO_2–54SiO_2$, and $35SrO–15TiO_2–45SiO_2$ glass systems of a fresnoite-type and concluded that the control of the chemical composition plays a critical role in achieving strong orientation and high optical transparencies necessary for the fabrication of functional optical materials.

Nevertheless, despite many advantages of transparent glass-ceramic materials and application potentials, transparent, fully crystallized ceramics are still worthy of consideration due to their application capacities, favorable characteristics, and availability of ceramic processing methods. Recently, a new approach has been proposed to fabricate transparent ceramics by the complete, congruent transformation of an amorphous body to the crystalline state [99, 100]. In other words, the material undergoes a complete transition from amorphous to polycrystalline state (in this case, amorphous refers to a non-crystalline glass, although the terms amorphous and glass should not be used completely interchangeably, as explained by Zanotto and Mauro [113]). According to the recently updated definition of glass-ceramics, a fully crystallized glass material in which available characterization tools (e.g., XRD or SEM) do not detect the presence of a residual glass phase (below the limits of detection) is considered ceramic, regardless of the materials processing technique applied for its fabrication. By contrast, if even the smallest amount of the glass phase is detected in the material after the crystallization, then the material should be considered glass-ceramic. Therefore, the exact definition can be applied to polycrystalline materials obtained via the full glass crystallization route, where a fully crystallized glass sample is called a ceramic as there is no more glass in the sample after the crystallization process. [102] One of the most significant advantages of the glass crystallization route for fabricating transparent ceramics is that it allows for final materials with very low porosity levels to be produced, as the original glass bodies have the ultra-low porosity levels typical of glass melting and forming processes, and this property can be retained in the resulting ceramics. Typically, the initial glass material exhibits very low porosity; therefore, the glass crystallization route does not pose the same technological challenges as conventional ceramic processing associated with eliminating all porosity as a prerequisite for achieving high optical transparency. However, the glass and crystalline phases

must show a limited density difference. It has been observed that the density difference between the glass and ceramic phases of up to a few percent typically results in the formation of high-density, i. e. low porosity ceramics. Currently, the available literature has not explained the reasons for thus behavior, and many questions in this regard remain unanswered. Nevertheless, opportunities exist for future work on this topic to address the observed phenomena. At temperatures above the glass transition temperature (T_g), glass materials may exhibit far more flexibility than, for example, a metal; consequently, glasses can accommodate various strains and internal stresses much more easily before grain boundary separation occurs. However, grain boundary separation may occur during glass crystallization if the density difference between the glass and crystal phase is too high. Moreover, the crystallized glass route completely circumvents issues associated with the addition of sintering additives that are required for conventional sintering processes, which include additive segregation at grain boundaries, and the formation of secondary phases. [114] In some cases, the glass crystallization route may even allow for the formation of ceramic materials with smaller grain sizes than those produced with conventional sintering techniques [115], as such techniques generally result in ceramics with micrometer-scale grains due to the high grain growth rates observed at the temperatures required for densification to occur. The temperature of glass crystallization, which occurs far below the sintering temperatures during conventional sintering, underpins the formation of very small crystallites and enables access to metastable phases that are otherwise difficult to obtain using the high-temperature and/or high-pressure powder sintering. Additionally, in anisotropic ceramic systems, birefringence effects [99] must be minimized to achieve acceptable transmittance levels, which can be engineered in various ways during glass crystallization. For example, Al Saghir et al. [116] increased the transparency of the crystallized $Sr_{1+x/2}Al_{2+x}Si_{2-x}O_8$ ceramics by controlling the degree of chemical disorder,

which induced structural disorder in the aluminosilicate network to lower the birefringence. On the other hand, in another study, the same group increased the optical transmittance of $BaAl_4O_7$ ceramics [117] by decreasing its birefringence through the deviation from nominal composition, which facilitated the formation of a secondary phase and inhibited the crystal growth of the main anisotropic phase via a Zener pinning effect.

Like the controlled crystallization of glass-ceramics from glass materials, the full glass crystallization of ceramics obeys the same principles of the theory of glass crystallization. The controlled formation of nuclei (nucleation) and their crystal growth (crystallization) are the most important steps of the fabrication process because they define the microstructure and transparency characteristics of the ceramics. Since both processes are very complex, this review will not engage in a detailed discussion on these topics; it will instead provide some theoretical basics and directions for further exploration. The readers are instructed to search many textbook references related to nucleation and crystallization in glasses. [118-120]

According to the classical nucleation theory, the thermodynamic driving force for nucleation and crystal formation is the change in the Gibbs free energy (ΔG) between the forming crystalline phase and the glass matrix. There are two types of nucleation processes: homogeneous and heterogeneous nucleation, which, as will be explained later on, can follow two nucleation mechanisms known as volume and surface nucleation.

The homogeneous nucleation assumes the formation of a nanometer-sized nucleus of a new phase resulting from the local fluctuations of density and kinetic energy. [118] When the Gibbs free energy change is negative, a supercritical nucleus forms with a critical radius (r^*):

$$r^* = -\frac{2\gamma}{\Delta g_V} \quad (8)$$

where Δg_V corresponds to the free energy change per unit volume caused by the formation of a nucleus. Nuclei that exhibit radii $r \geq r^*$ can continue their growth into larger crystals; by contrast, nuclei with radii $r < r^*$ cannot continue their growth and eventually dissolve back into the glass matrix. The resulting critical Gibbs free energy of the homogeneous nucleation (ΔG^*_{HOM}) is determined according to the equation:

$$\Delta G^*_{HOM} = -\frac{16\pi\gamma^3}{3(\Delta g_V)^2} \quad (9)$$

The second nucleation type – heterogeneous nucleation, much more common than the homogeneous, requires the presence of external surfaces or impurity interfaces as nucleation catalysts that are different from the glass matrix. [118] In systems undergoing heterogeneous nucleation, the nucleation catalysts create a much stronger driving force towards the glass → crystal phase transformation than the glass matrix alone, which is why in this phenomenon, the interaction between different interfaces and their surface energies plays a critical role. Therefore, the critical Gibbs free energy of heterogeneous nucleation (ΔG^*_{HET}) can be expressed as a function of the contact angle (θ) between the forming nucleus (with a shape of a spherical cap) and the catalyst's surface:

$$\Delta G^*_{HET} = \Delta G^*_{HOM} f(\theta) \quad (10)$$

with the factor $f(\theta)$ defined as $f(\theta) = (2 + \cos(\theta))\,(1 - \cos(\theta))^2 / 4$.

Which of the two nucleation paths will control the crystallization in the glass material during the full glass crystallization is a matter of the material's composition and the processing steps, including the glass treatment conditions and processing technique used. Furthermore, the kinetics of the nucleation process is a time function of two parameters, regarded at the nucleation rate (I) and the nucleus number (N). The steady-state nucleation rate (I) that defines the number of nuclei of a critical radii r^* formed per unit volume and time is expressed as [118]:

$$I(t) = I_0 \, exp\left(-\frac{\tau}{t}\right) \quad (11)$$

whereas the nuclei number (N) formed in the time interval (t) and after an incubation time (τ) can be derived by integrating I:

$$N = \int_0^t I(t) \, dt \quad (12)$$

Additionally, the precipitation of a new phase from the glass matrix can follow two possible mechanisms known as the volume nucleation and surface nucleation, which are functions of many factors including glass composition, stoichiometry, presence of (heterogeneous) nucleating agents, phase separation processes, processing techniques and conditions, and others. The mechanism of volume nucleation involves the precipitation of nuclei in the volume of the parent glass, which is the most common nucleation process in glasses. By contrast, surface nucleation, as implied by its name, occurs at the glass surface and is a less common mechanism among the known glass systems. Moreover, it is more difficult to control since the factors causing surface nucleation are not fully understood yet.

Once the formed nuclei reach the critical size (r^*), the glass system enters the crystal growth phase that involves the material transport to the nuclei's surface, allowing them to grow further. At this point, the kinetics of the growth process is controlled by the rate of atom diffusion and interface reactions between the nuclei and the glass matrix surrounding the nuclei, whereas the characteristics of the final product are defined by the shape and size of the crystalline phase and its microstructure. [120]

Concerning the mechanism through which the formed nuclei continue their growth, three growth models are identified: normal growth, screw dislocation growth, and surface crystallization growth. [118] In the case of the normal growth model, the crystal growth rate (V) presented by the following relation:

$$V = \nu a\left(1 - exp\left(-\frac{\Delta G}{kT}\right)\right) \quad (13)$$

is defined by the frequency factor (υ) of material transport to the rough nuclei surface and the Gibbs free energy change (ΔG). Similarly, the screw dislocation growth mechanism uses the exact approximation but expands it with a factor *f* that considers the number of possible dislocation sites for the atom attachment. Lastly, the surface crystallization growth mechanism assumes the material attachment to the smooth nuclei surface and is defined by the following relation:

$$V = C \cdot \nu\, exp\left(-\frac{B}{T \cdot \Delta T}\right) \quad (14)$$

where *C* and *B* represent the time-function parameters.

Phase separation in the form of droplets of a denser disordered phase in a glass matrix, initiated either by a liquid-liquid separation or critical density fluctuations, is one of the fundamental phenomena governing nuclei precipitation. For example, forming a network modifier-rich phase can significantly reduce the diffusion enthalpy, aiding the nucleation process. [121] The formed high-density droplets represent the precursors for the structural ordering and nucleation. [120] Therefore, the structure of the glass melt and its thermodynamic characteristics, including the system's free energy controlling the melt's homogeneity, play a critical role in whether the phase-separation phenomenon will occur. The size of the phase-separated droplets formed initially inside the glass matrix limits the size to which the crystallites will grow. [122] More importantly, the size of the crystallites defines the degree of transparency of ceramics at the end of the crystallization process. Therefore, controlling the droplet size in glasses exhibiting phase separation is essential in retaining the material's transparency.

Complete removal of the glass matrix is a prerequisite for the ceramics produced via full glass crystallization. However, in many cases, the controlled full glass crystallization is quite complex, and often it results in the formation of crystals of various types or even crystal phases (e.g., biphasic

ceramics [117]). The task becomes even more complex when the crystallized glasses are expected to transform into highly-transparent ceramics.One of the most significant challenges in current transparent ceramic processing technology is the large-scale fabrication of homogeneous bodies, as explained by Ikesue et al. [3] in their discussion on ceramic laser gain media. The crystallized glass route for producing transparent ceramics is a promising alternative for overcoming these challenges, as it utilizes the scalability of glass-forming processes. Additionally, the shape restrictions imposed by traditional ceramic forming techniques can theoretically be overcome, expanding shaping capabilities to those of well-established glass forming techniques.

The current literature concerning the production of transparent ceramics by the glass crystallization route includes a number of reports that detail several different methods by which the process can be conducted. Although each of these reports details a different approach for parent glass preparation, the overarching principle is the same: to take a glass and convert it into a fully crystalline ceramic specimen. Of note, this field of research is relatively new, and most of the understanding of this novel approach for transparent ceramic fabrication has come from limited experimental data. Therefore, this review aims to spark interest and encourage researchers from different fields and backgrounds to enhance knowledge and provide a better theoretical basis for explaining the phenomena underlying full glass crystallization.

5. Techniques for the fabrication of transparent ceramics by crystallization from glass

5.1 Melt-solidification technique

Some of the earliest reports (Araki et al., 2004 and 2006 [123, 124]) on the glass crystallization route for making transparent ceramics are by the annealing of glasses obtained by melt-solidification. The melt-solidification technique involves melting a powder mixture pellet on a water-cooled copper plate by focused radiation from a xenon lamp followed by a solidification into a transparent spherical bulk specimen. The spherical shape of the obtained samples results from the surface tension of the melts. The cooling rates observed during melt-solidification are in the 200–500 K/s range [124], which allows the fabrication of bulk samples with a few millimeters in diameter. The formation of amorphous glass bulk is achieved by quenching the metastable liquid phase upon cooling of the eutectic melt. After the glass is formed, it is subjected to an annealing treatment at a temperature far below the ceramic sintering temperature to initiate crystallite formation.

The melt-solidification technique is a fairly well-established route for glass preparation, with the approach having been applied successfully in the context of the glass crystallization route [124] to form glasses from eutectic melts of so-called network former oxides (e.g., SiO_2, B_2O_3, P_2O_5, etc.). However, it was also demonstrated that the technique enables glasses to be produced from solidified eutectic melts in ternary or multiple phase systems without the incorporation of any network former oxides. Subsequent annealing treatment of these compositions, such as HfO_2–Al_2O_3–$GdAlO_3$ glass, under varying temperature and time conditions, produced transparent nano-composite ceramic samples with optical transmittance levels similar to that of the parent glasses (**Figure 5(a)–(d)**). It was observed that samples with partial or even complete crystallization from the glass phase could be obtained, depending on the annealing regime. TEM and XRD studies revealed that annealing at 1000°C resulted in the precipitation and growth of fluorite-structured hafnia crystals only 5–10 nm in size. In contrast, annealing at 1200°C resulted in the nucleation

and growth of both hafnia and cubic perovskite crystalline phases. Annealing at temperatures above 1200°C produced full crystallization and resulted in the formation of a secondary gadolinium aluminum perovskite ($GaAlO_3$) phase beyond the cubic hafnia. The resulting ceramics was a nanocomposite with crystallite sizes sufficiently large to decrease the optical transparency (50–100 nm) (**Figure 5(e)–(f)**). Nonetheless, the result demonstrated that the approach has the potential for producing transparent nanocrystalline ceramics of multiple-phase systems without network former oxides included if the process could be optimized to obtain full crystallization while minimizing crystallite size to acceptable values.

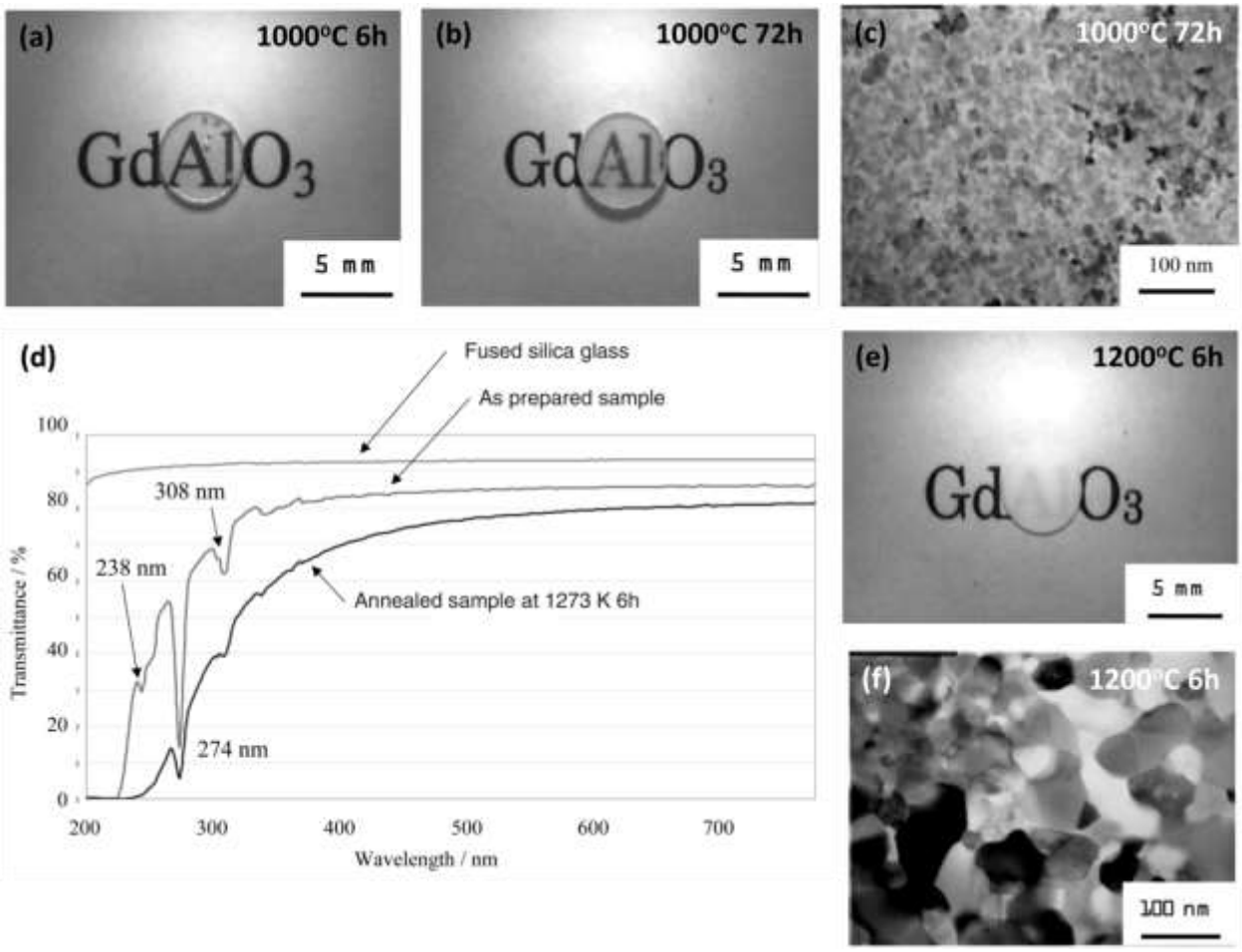

Figure 5. (a), (b), (e) Photographs and (c), (f) TEM micrographs of HfO_2–Al_2O_3–$GdAlO_3$ samples annealed at different temperatures and times; (d) Optical transmission spectra of the parent glass and annealed ceramic samples. [123]

5.2 Aerodynamic levitation technique

Another technique that has drawn significant research attention for the fabrication of transparent ceramics is the annealing of millimeter scale glass beads produced using the aerodynamic levitation (ADL) method. The original aerodynamic levitator design by Paul C. Nordine and his group [125] was developed for studying gas/liquid reaction rates and gasification kinetics in both solid and liquid samples, for a variety of applications such as steelmaking, catalysis, combustion,

etc. [126] The setup was later redesigned by a research group at the CEMHTI laboratory in Orléans, France for experimental work on glass beads. The redesigned instrument (**Figure 6**) used a gas stream (e.g., Ar, He, N_2, or O_2, or gas mixtures, such as O_2/N_2, N_2/H_2, or O_2/Ar) to levitate a single powder pellet, which is heated and melted by radiation from two CO_2 lasers. The molten material is then solidified into a glass bead by rapid containerless cooling of the order of a few hundreds of $^oC/s$ (cooling rates depend on the bead size, composition, gas nature, etc.), which is initiated by simply terminating laser heating, which results in heat being rapidly lost by conduction to the flowing gas stream. The system was unique in its capability to cause uniform melting and quenching of the material under contactless/containerless conditions. Subsequent annealing of the glass bead under appropriate temperature and time conditions initiated the full, congruent crystallization of the amorphous glass into a polycrystalline body with thin grain boundaries. In addition to the advantages of the glass crystallization approach mentioned earlier, the ADL method provides a couple of other benefits, such as (1) enabling conditions suitable for the fabrication of transparent ceramic (metastable) phases that could not otherwise be prepared via conventional sintering techniques, such as materials with non-cubic symmetries; (2) application of CO_2 lasers that ensure homogeneous heating and melting at temperatures up to 3000^oC; (3) contactless/containerless processing that avoids contamination from the crucibles and heterogeneous crystallization; (4) access to fast cooling rates arising from the containerless conditions that can be tuned based on the nature (primarily mass) of the gas used ($Ar < O_2 < He$).

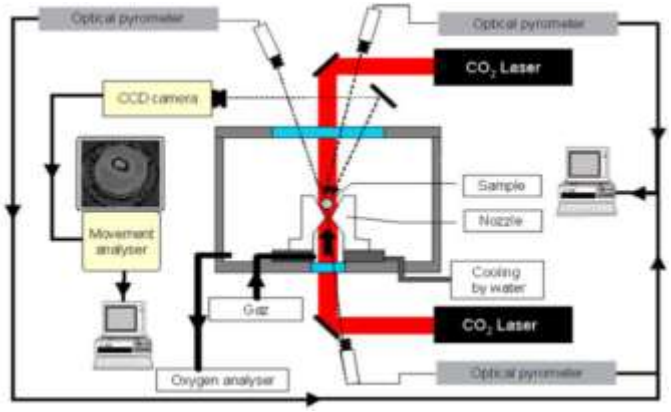

Figure 6. Schematic representing aerodynamic levitation (ADL) system. [99]

In 2012, Allix et al. [99] reported the fabrication of $BaAl_4O_7$ transparent ceramics by full crystallization of a glass bulk synthesized by ADL method. Two orthorhombic polymorphs, α-$BaAl_4O_7$ and β-$BaAl_4O_7$, which structures were determined and illustrated with the models in **Figure 7(a)**, could be isolated at different annealing temperatures for this new ceramic composition. Both ceramics exhibited good visible-range transmittance (**Figure 7(b)**), minimal porosity, and very thin grain boundaries. The report was particularly notable due to the observation that despite the fabricated ceramics exhibiting micrometer-scale grain sizes, they retained a high level of transparency, an observation that contradicts the general expectation that high transparency levels are only possible in ceramics with nanoscale grains. The report highlighted multiple aspects of the utility of the ADL method for the fabrication of transparent ceramics. First, the method enabled $BaAl_4O_7$ phases to be produced that are unattainable using a solid-state reaction approach, due to compositional instability at high temperatures. Second, the approach enabled the fabrication of anisotropic transparent ceramics with birefringence of around 0.01 calculated using the density functional theory (DFT); a feat that is significantly challenging using traditional techniques.

Subsequent to their 2012 report on the conversion of glass to ceramic via the aerodynamic levitation and annealing approach, the Allix group employed the same approach to fabricate transparent ceramics of other compositions in which the structural, optical, scintillation, and other properties of the ceramics were investigated. One composition was cubic $Sr_3Al_2O_6$ [100], where the produced ceramic exhibited low porosity levels similar to the starting glass, and optical transmittance levels in the visible and infrared (IR) range that approached theoretical values. The technique was also effective in producing transparent ceramics with tetragonal symmetry in the melilite family with the general formula of ABC_3O_7, where the specific compositions investigated were Sr*RE*Ga_3O_7, with *RE* = Eu, Gd, Tb, Dy, Ho, Y, Er, Tm, and Yb. [127] In a subsequent study on Eu^{2+}-doped $BaAl_4O_7$–$BaAl_2O_4$ biphasic ceramics with notable scintillation properties [117, 128], the same authors determined that transmittance levels could be increased by increasing the initial concentration of BaO in the glass precursor powder mixture. Increasing the BaO content facilitated the spontaneous formation of a secondary $BaAl_2O_4$ phase, which formed from the Ba-rich residual glass matrix after crystallization of $BaAl_4O_7$. As shown in the TEM micrographs in **Figure 7(c)**, the resulting microstructure comprised of micrometer-sized $BaAl_4O_7$ grains (1.4–7.2 μm, depending on the glass composition) and spherical $BaAl_2O_4$ nano-crystallites (20–30 nm) formed within the $BaAl_4O_7$ grains. According to the schematic presented in **Figure 7(d)**, the crystallization mechanism involves the embedding of $BaAl_2O_4$ nano-sized grains into $BaAl_4O_7$ grains as a result of the formation of the secondary phase particles at the grain boundaries of the primary phase. Due to their very small size, these secondary crystallites did not contribute to light scattering. Moreover, they limited the growth of the main $BaAl_4O_7$ phase via a Zener pinning effect, making the biphasic ceramics more transparent than the single-phase birefringent $BaAl_4O_7$ ceramics, which exhibited a larger average crystallite size and correspondingly higher

birefringence. The ceramics obtained in this study represent the first report in which the novel biphasic transparent ceramics were elaborated by full crystallization from glass.

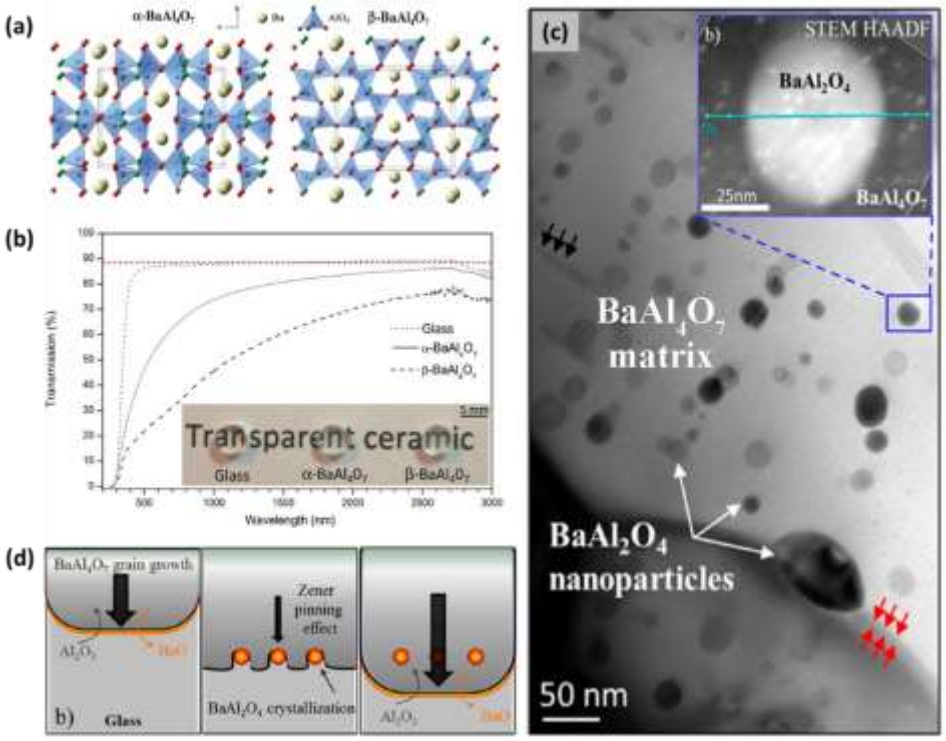

Figure 7. (a) Model crystal structures of α-$BaAl_4O_7$ and β-$BaAl_4O_7$ polymorphs and (b) photograph and optical transmittances of the $BaAl_4O_7$ parent glass and corresponding ceramics; [99] (c) TEM micrograph of the $BaAl_4O_7$ ceramic matrix with dispersed $BaAl_2O_4$ nano-sized crystallites and (d) schematic depicting the proposed crystallization mechanism in the $BaAl_4O_7$–$BaAl_2O_4$ biphasic transparent ceramics. [117]

In another study from the same authors, the first-ever anionic conducting transparent ceramic was reported, a melilite phase with the composition of $Ln_{1+x}Sr_{1-x}Ga_3O_{7+\delta}$ (Ln = Eu, Gd, Tb; $0.4 \leq x \leq 0.6$) [129] that has brought several important factors associated with the glass crystallization via the ADL technique together. Firstly, the use of the ADL technique as an alternative method to the solid-state synthesis, enabled the authors the formation of a new metastable phase (Ln = Tb, $x = 0.4$) with charge carriers present only because of the low-temperature synthesis; and secondly, the high transparency of $Ln_{1+x}Sr_{1-x}Ga_3O_{7+\delta}$ ceramic samples,

underpinned by extremely low porosity, simultaneously aided the ionic conductivity of the ceramics by lowering grain boundary resistance. Later on, driven by the potential of the ADL technique to produce fully crystalline transparent melilite ceramics of different compositions and structures starting from the glass, interesting for solid oxide fuel cell devices and other novel applications, the authors continued the research and presented comprehensive studies on the structural and physical properties of a several metastable ceramics compositions, including transparent rare-earth gallate ($Sr\mathit{RE}Ga_3O_7$, *RE* = Dy–Lu, Y, [130]), and aluminate ($La_{1+x}Ca_{1-x}Al_3O_{7+0.5x}$, $0 \leq x \leq 0.5$) [131] and gallate ($La_2Ga_3O_{7.5}$, $x = 1.0$) [132] melilite ceramics. The last two reported ceramics demonstrated once again the chemical and structural diversity of the fully crystalline ceramic materials that can be obtained via the ADL technique. Moreover, Wisniewski et al. [133] tried to elucidate the growth mechanism in the $La_2Ga_3O_{7.5}$ glass-ceramic beads obtained via the ADL method in a search for the link between the experimental conditions during crystallization (e.g., cooling profiles) and the material's transparency, which could potentially enable fabrication of single crystals of metastable phases using this novel technique.

Another study from the Allix group reported the fabrication of undoped and Eu^{2+}-doped $Sr_{1-x/2}Al_{2-x}Si_xO_4$ ceramics by the glass crystallization method, with the ceramics being reported as promising for next-generation integrated light-emitting devices due to their high density, low porosity, and highly oriented birefringent crystals. [134, 135] In the following study, the authors reported hexagonal Eu^{2+}, Dy^{3+}:$Sr_{1-x/2}Al_{2-x}Si_xO_4$: ($0.1 \leq x \leq 0.5$) transparent ceramics [136] prepared using the same approach, which exhibited persistent tunable luminescence from blue light to green that could last for even several tens of minutes by charging the ceramics with just a low-power LED source. More importantly, throughout these studies, a relationship between the composition of the glass beads prepared via the ADL method and the crystallization mechanism has been observed;

the resulting microstructure during the annealing step should be further studied to determine correlation between the design and the properties of transparent ceramics. In some materials, depending on the initial glass composition, glass crystallization starts from the surface of the glass bead. In a prior study [135], subtle SiO_2 content variations in the $Sr_{1-x/2}Al_{2-x}Si_xO_4$ glass system (x = 0.9, 0.7, and 0.5) have been found to result in an oriented nucleation and crystal growth at the glass surface that does not continue to follow the same trend with further growth of grains in bulk parts of the glass pieces. **Figure 8** presents the EBSD images of the three glass compositions from that study, showing samples with Sr content of 0.55 and 0.65 (Sr = 1-x/2) exhibiting a relatively homogeneous distribution of grain orientations in the bulk parts, and a sample with Sr = 0.75, displaying a unique crystallographic texture with some degree of orientation deviation (~30°), thus indicating the existence of a completely different crystallization mechanism from that in the first two samples. In contrast, glass crystallization in other materials is not necessarily limited to the glass surface. Nucleation and crystal growth can appear more homogeneously distributed throughout the sample's volume, whereas in other cases (e.g., aluminate glasses), they may occur so rapidly that the intermediate stages of crystallization cannot be observed *in situ*.

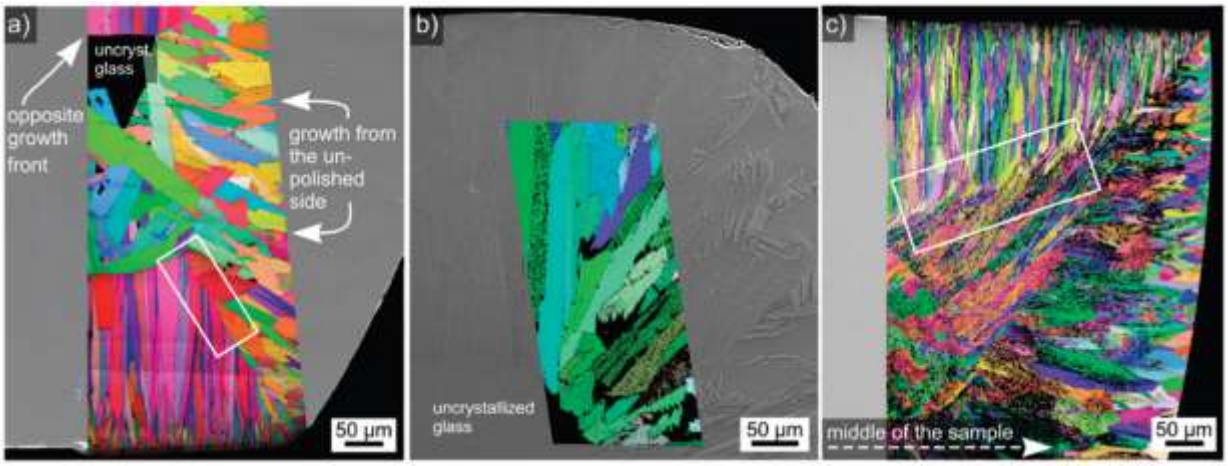

Figure 8. Inverse pole figures (IPF) of the EBSD scans of $Sr_{1-x/2}Al_{2-x}Si_xO_4$ glasses with Sr content of (a) 0.55, (b) 0.65, and (c) 0.75, displaying the changes in the crystal growth directions between the surface and bulk. [135]

Beyond the previous reports, a collaboration between the previous authors and the Li group [137], has resulted in a study on the fabrication of YAG–Al_2O_3 transparent composite ceramics by using the ADL and annealing approach. The biphasic pore-free ceramics obtained via complete crystallization from the glass phase exhibited mechanical properties superior to YAG single-crystals and conventionally-derived ceramics. Despite the substantial difference in the refractive indices between Al_2O_3 (n = 1.60) and YAG (n = 1.82) phases, the ceramics exhibited high optical transparency levels in the visible-near IR wavelength range, owing to the nanometer-sized YAG and Al_2O_3 grains, which greatly minimized light scattering (**Figure 9(a)**). TEM analysis of the sample's microstructure revealed the presence of both YAG and Al_2O_3 phases, which were easily discerned as dark and light areas in the micrographs, respectively, owing to the different average atomic numbers (Z) of the two phases (**Figure 9(b)**). The results also indicated that the thin Al_2O_3 barriers surrounding the 3-D network of YAG grains played a major role in limiting the growth rate of YAG grains, even at high temperatures, and were the main contributors to the nanocrystalline structure and high optical transmittance of the ceramics. Finally, investigation of the effect of Ce^{3+} doping on the YAG–Al_2O_3 nanoceramics has demonstrated that quantum efficiency levels comparable to those of commercial Ce^{3+}:YAG single-crystals can be achieved.

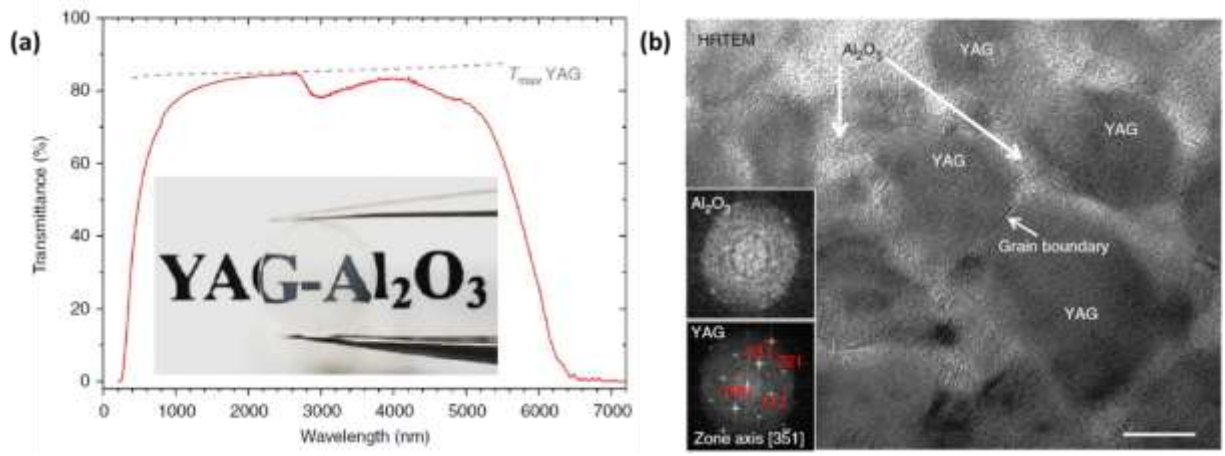

Figure 9. (a) Transmission spectrum and photograph, and (b) high-resolution TEM micrograph confirming the co-existence of two crystalline phases (YAG and Al_2O_3) in YAG–Al_2O_3 transparent ceramics obtained by full crystallization from the glass phase. [137]

Further on, in the most recent study [138], the group conducted a comprehensive experimental analysis of the non-isothermal crystallization kinetics in the biphasic YAG–Al_2O_3 system to gain a better insight into the crystallization mechanism of their highly transparent YAG-based nanoceramics. Additionally, the same group also demonstrated how the limits in the size of the samples prepared via the ADL method could be overcome by sintering the powder of the crushed ADL-prepared glass beads in a hot-press sintering furnace to obtain larger sized (~10 mm in diameter) glass samples at relatively low temperature and low pressure. Although not fully crystallized, the authors obtained highly transparent bulk La_2O_3–TiO_2 glass samples with the addition of a very small amount of SiO_2 as an additive that simultaneously suppressed the crystallization and aided the glass-forming ability. [139] Similar results were also observed in two other systems, La_2O_3–Nb_2O_5 [140] and La_2O_3–TiO_2–ZrO_2 [141], where the transparent glass samples of larger size and high density were obtained as a result of the plastic flow mechanism during the hot-press sintering.

5.3 Melt-quenching technique

Although a number of techniques exist for producing transparent ceramics via the crystallized glass route, likely the simplest involves the use of the melt-quenching technique (as it is most commonly known in the literature), to produce a parent glass, followed by an annealing treatment to crystallize the glass into ceramic. The melt-quenching method involves the preparation of a glass by fusion of a powder mixture in a crucible, followed by quenching to room temperature with a relatively slow cooling rate (not by ultra-fast quenching). Subsequently, full glass crystallization is achieved by subjecting the glass to an appropriate annealing heat treatment. Annealing treatments can be conducted above or below the glass transition temperature (T_g) of the material, with certain treatments performed below T_g in order to relieve the internal stresses generated during thermal quenching. The approach holds multiple advantages over conventional ceramic processing routes, including the ability to produce ceramics with chemical compositions unobtainable via conventional ceramic sintering techniques, as well as high cost-effectiveness, high scalability, and high shape versatility.

Al Saghir et al. [116] used the melt-quenching approach to produce single-phase $Sr_{1+x/2}Al_{2+x}Si_{2-x}O_8$ ($0 < x \leq 0.4$) transparent ceramics by full congruent crystallization from the parent glass. Optical transmittance levels of ~90% were obtained in the visible and near-IR ranges; a value that approaches theoretical levels (**Figure 10(a)**). The results were noteworthy in that excellent optical properties were obtained despite the material having hexagonal symmetry and exhibiting micron-sized crystallites (5–20 μm), with the behavior attributed to very low porosity levels, very thin grain boundaries (**Figure 10(b)**), and low birefringence, with the latter being achieved by controlling chemical disorder within the material's structure. Notably, the ceramic

surface structure comprised of crystallites oriented perpendicularly to the surface (**Figure 10(c)**), because of the heterogeneous surface nucleation, which also helped to decrease the birefringence effect and promote transparency.

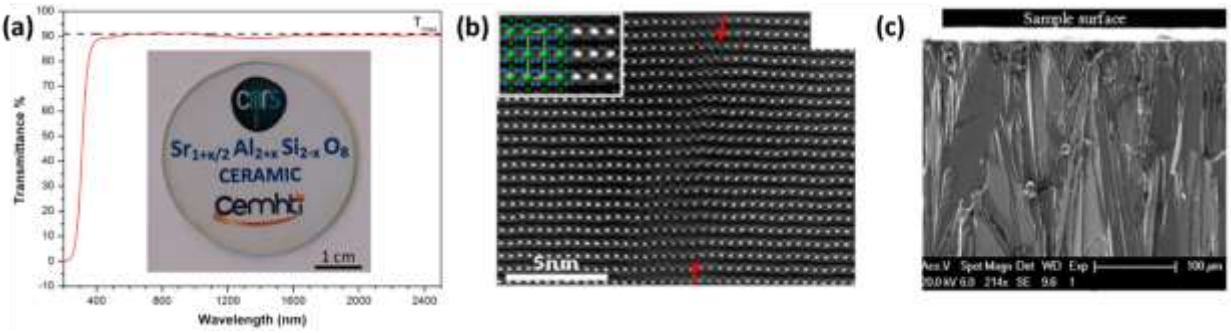

Figure 10. (a) Photograph and optical transmittance spectrum, (b) high-resolution TEM micrograph taken at the interface between grains (red arrows emphasize the location of the thin grain boundary), and (c) SEM micrograph depicting the crystal growth oriented perpendicularly to the surface of $Sr_{1+x/2}Al_{2+x}Si_{2-x}O_8$ (x = 0.2) transparent ceramics. [116]

A later study by Bertrand et al. [101] confirmed that full crystallization from the glass phase could be applied to the fabrication of tellurite-based transparent ceramics with the general formula of $ABTe_3O_8$; specifically $Bi_{0.8}Nb_{0.8}Te_{2.4}O_8$. The report detailed the first-ever cubic ceramics with this composition, which exhibited a large optical window from 0.5 µm to 5 µm with ~74% transmittance in the 3–5 µm range, and excellent mechanical properties (e.g., hardness, Young's modulus). Similarly to Al Saghir's report, the good optical properties were attributed to the lack of light scattering sources (high-density and pore-free structure, very thin grain boundaries, and the absence of amorphous phase with different refractive index). In another report on the same tellurite-based ceramics, Dolhen et al. [142] demonstrated their laser properties. The report emphasized the critical importance of the parameters of the crystallization step, with the observations that annealing temperature and time had a substantial influence on both the formation of the cubic $Bi_{0.8}Nb_{0.8}Te_{2.4}O_8$ phase, as well as the grain size (3–5 µm) of the ceramics, which

ultimately determined optical transmittance. A slight reduction in optical transmittance was observed with an increase in annealing time from 5 to 15 min, as can be observed in the spectra shown in **Figure 11(a)**. The addition of Nd^{3+} dopant was observed to cause a slight decrease in transmittance to occur. In terms of laser performance, the fabricated Nd^{3+}-doped tellurite ceramics exhibited an output power of around 28.5 mW in continuous wave mode, a laser efficiency of approximately 22.5%, and slope efficiency of nearly 50%; values on the same order as reported for other tellurite laser materials. The latest report from the group at the Institute of Research for Ceramics (IRCER), Limoges, France [143] details a study on a model tellurite glass that attempts to develop a fundamental understanding of the crystallization process. It was concluded that the glass to crystal transformation process occurs by transition of the (transparent) $Bi_{0.8}Nb_{0.8}Te_{2.4}O_8$ parent glass to an intermediate anti-glass phase (translucent), and then by a subsequent transformation to the target crystalline phase (transparent). XRD has indicated that the transitioning anti-glass phase and the high-temperature ceramic phase are two polymorphs, the first indexed as β-$Bi_2Te_4O_{11}$ and the second indexed as the phase isostructural to MTe_3O_8 (M = Ti, Zr, Hf, Sn). Further EBSD analysis has revealed that both the anti-glass and ceramic phases appear fully crystallized (**Figure 11(b)**); however, the complete structural ordering does not occur until the higher temperature is achieved, thus indicating the anti-glass → ceramic phase transition. The partial ordering of the anti-glass phases has been demonstrated to be a complex structure consisting of larger domains (~700 nm) comprising smaller domains (~50 nm), as shown in the TEM micrographs in **Figure 11(c)**. The ceramic phase exhibits a similar microstructure comprised of larger grains of ~2 μm and ~8 μm, depending on the annealing time, as well as smaller grains (**Figure 11(d)**). However, despite the general understanding that the glass crystallization route yields transparent ceramics free of porosity, the produced ceramic pieces exhibit some porosity,

probably because of the density difference between the glass (6.00 g/cm^3), anti-glass (6.20 g/cm^3), and ceramic phases (6.27 g/cm^3). In contrast, the porosity does not appear to affect the ceramics' transparency and lasing performance, because of the sufficiently small pore size of approximately 20 nm.

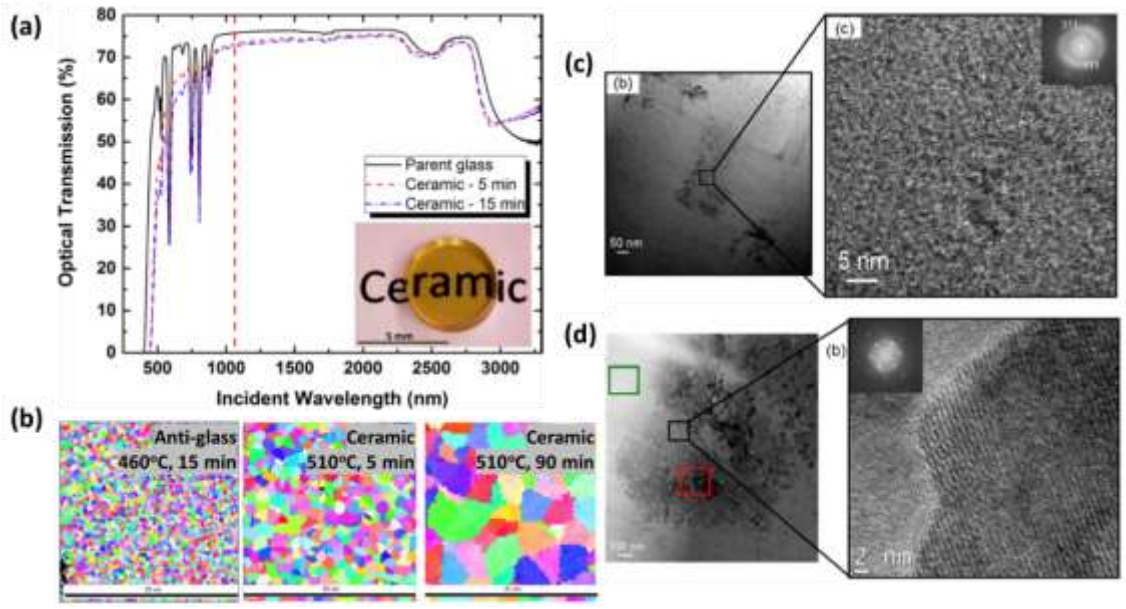

Figure 11. (a) Photograph and optical transmittance spectra of transparent Nd^{3+}-doped $Bi_{0.8}Nb_{0.8}Te_{2.4}O_8$ tellurite ceramics obtained by annealing at 510°C for 5 min and 15 min; [142] (b) EBSD images of anti-glass and two transparent ceramic samples of $Bi_{0.8}Nb_{0.8}Te_{2.4}O_8$ composition, obtained via the melt-quenching method; TEM and high-resolution TEM micrographs of (c) anti-glass and (d) ceramic samples in (b). [143]

Recent reports on the glass crystallization method for making transparent ceramics have sought to develop an understanding of the fundamental principles of the process. In a report by Wen et al. [115] investigating the crystallization of melt-quenched tellurite-based ceramics bulk glass and glass fibers, the authors were able to tune crystallite size from nanometer-scale to micron-scale by achieving control over crystallite nucleation and growth by following their predictions illustrated in the schematic in **Figure 12(a)**. The schematic represents a pathway for the fabrication of highly transparent nanoceramics, which can be achieved by inducing nucleation and suppressing the

growth process in the material. The authors determined that Bi_2O_3 acts as a network modifier in the system and serves to promote crystallization, with variation of the starting Bi_2O_3 content significantly affecting nucleation and growth processes. Samples with lower Bi_2O_3 levels exhibited grains as large as 20 μm (**Figure 12(b)**), while those with greater relative Bi_2O_3 contents exhibited grains as small as 20 nm (**Figure 12(c)**). The relationship between Bi_2O_3 content and grain size was observed in both ceramic bulk and fiber samples, and was reflected in material properties, with Bi_2O_3-rich samples exhibiting superior mechanical, optical (**Figure 12(d)** and **Figure 12(e)**), and laser properties, due to their reduced grain sizes.

In a study by Qiang et al. [144] that investigated the ceramic phosphor Eu^{2+}:$Sr_{1.1}Al_{2.2}Si_{1.8}O_8$ as a candidate material for white LED light applications, it was observed that subjecting the samples to an annealing treatment resulted in the formation of a ceramic-glass-ceramic multilayer composite structure, with crystallization occurring only at the exterior of the glass body, and the inner portion remaining in the glass state. Additionally, it was observed that the annealing time of the parent glass had a notable influence on the formation and thickness of the crystalline layers of the composite. The annealed specimens contained both amorphous and crystalline phases, with the crystalline phase consisting of highly *c*-axis oriented grains, which allowed for high optical transmittance to be achieved despite being optically anisotropic.

Finally, the most recent 2022 report by Tang et al. [145] worth mentioning in this section reported on the highly-crystalline transparent monoclinic $Ba_5Si_8O_{21}$ composite ceramics obtained by full crystallization of melt-quenched $37.5BaO–62.5SiO_2$ glass. The Eu and Ce ions doped scintillation ceramics exhibited high optical transparency and excellent mechanical and scintillation properties with the scintillating light yield of ~2.5 times higher than the commercial $Bi_4Ge_3O_{12}$ single-crystal,

which once again provided a proof of concept and application potential for this novel ceramic fabrication approach.

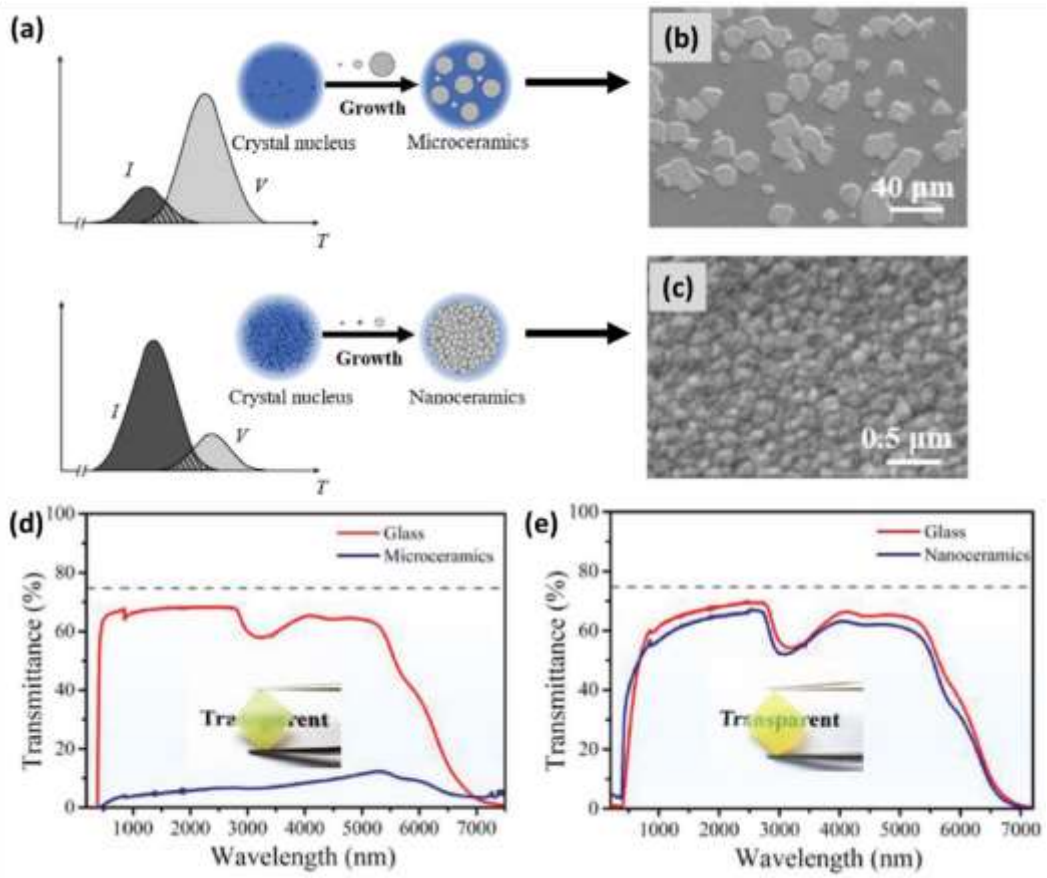

Figure 12. (a) Schematic suggesting the adjustments in the nucleation (*I*) vs. growth (*V*) rate curves for suppressing (top) or enhancing (bottom) the nucleation process; (b) and (c) SEM images of $Bi_{0.8}Nb_{0.8}Te_{2.4}O_8$ microceramics and nanoceramics, respectively, obtained on the basis of the models in (a). Optical transmission spectra and photographs of $Bi_{0.8}Nb_{0.8}Te_{2.4}O_8$ tellurite ceramics with (d) micron-scale and (e) nanometer-scale grains. [115]

5.4 Amorphous Sintering and Controlled Crystallization (ASCC)

One of the key requirements for achieving acceptable optical properties in transparent ceramics, especially those with anisotropic crystal structures, is to use techniques and strategies for their

fabrication that compensate for birefringence effects or that allow for nanometer-scale grain sizes to be achieved. However, the low nucleation rates and high grain growth rates typically observed at the temperatures required to densify ceramic materials make this very difficult to achieve. As such, it was proposed by Mei et al. that an effective route for the fabrication of nanoceramics would be one that allows for independent control of the densification and grain growth processes. [146] The proposed approach, which the authors termed "Amorphous Sintering and Controlled Crystallization" (ASCC), was intended to circumvent the challenges associated with achieving densification while minimizing grain growth. The ASCC method involves the preparation of glass microspheres by direct exposure of spray-dried spherical particles to flame (> 3000^{o}C), followed by extremely fast thermal quenching (~1000^{o}C/s) of the melted particles in water. The microspheres are then collected, dried, and used as a feedstock material for hot-pressing. After sintering at high temperature and under an applied load, a densified glass specimen is produced, which is then finally subjected to pressureless heat-treatment to initiate crystallization of the glass into a polycrystalline nanoceramic. The method utilizes viscous flow initiated by the applied load of the hot-press to effectively densify the glass microsphere powder into a bulk glass. The sintering process is conducted within a narrow temperature range above T_g but below the crystallization onset temperature (T_s). By this method, a dense ceramic can be produced by annealing at lower temperatures, where grain growth rates are minimal.

A first-ever mention of the transparent ceramic fabrication approach that fits the description above was by Rosenflanz et al. in 2004 [98], which was also one of the first reports discussing the glass crystallization route as a method of obtaining nanoceramics and bulk oxide glasses in systems that do not include classical glass formers. In this study, the authors demonstrated a quite novel fabrication approach by which they prepared fully crystallized transparent nanoceramic samples

by pressing the Al_2O_3–RE_2O_3 and Al_2O_3–RE_2O_3–ZrO_2 (*RE* = La, Gd, and Y) flame-spray-obtained glass microbeads into pellets and heat-treating them under pressureless and pressure-assisted conditions. Besides excellent mechanical and optical properties, the obtained ceramics also demonstrated the possibility of obtaining nanoceramics without the necessity of applying extremely high pressures during sintering (e.g., 1 GPa or higher) because of the simultaneous crystallization and grain growth during the heat treatment.

The years after, the term ASCC was proposed and discussed in more detail by Mei et al. in their 2011 report [146], describing its application to produce transparent ceramics of $LaAlO_3$; a composition that is otherwise very difficult to prepare as glass and to achieve transparency in ceramics due to its non-cubic symmetry and very high birefringence. In addition to the constituent oxides of the $LaAlO_3$ phase, ZrO_2 was added to the precursor mixture as a nucleation agent. An overview of the employed process is depicted in the diagram presented in **Figure 13(a)**. Precursor powder granules, previously prepared via the spray-pyrolysis method, were subjected to an C_2H_2/O_2 flame with a combustion temperature of around 3200^{o}C, which formed completely transparent glass microspheres upon quenching into a water bath (**Figure 13(b)**). During subsequent hot-pressing of the microsphere powder, the application of high pressure was determined to be essential in achieving effective densification, as it promoted the elimination of grain boundaries through viscous flow. However, some residual pores persisted throughout hot-pressing. In line with other studies, the report emphasized that the final crystallization heat treatment is the most sensitive step in the procedure, as the process parameters control the product ceramic grain size, which in turn dictates optical transparency. It was observed that annealing at 1200^{o}C for 2 h produced a fully crystallized and transparent $LaAlO_3$ nanoceramic (**Figure 13(c)**) with an average grain size of 40 nm, an IR-range optical transmittance of ~70%, and mechanical

properties superior to the parent glass. In a subsequent report by the same authors [147], the effect of pressure during the hot-pressing crystallization step was investigated in detail. SEM images of the parent glass microstructures obtained under different loading pressures are shown in **Figure 13(d**). It was also demonstrated that the ASCC approach can be applied to produce high optical quality transparent nanoceramics in other material systems, including 1.5% Er:$LaAlO_3/ZrO_2$, 1% Nd:YAG/HfO_2, and 3% Nd:YAG/HfO_2 (**Figure 13(e)**).

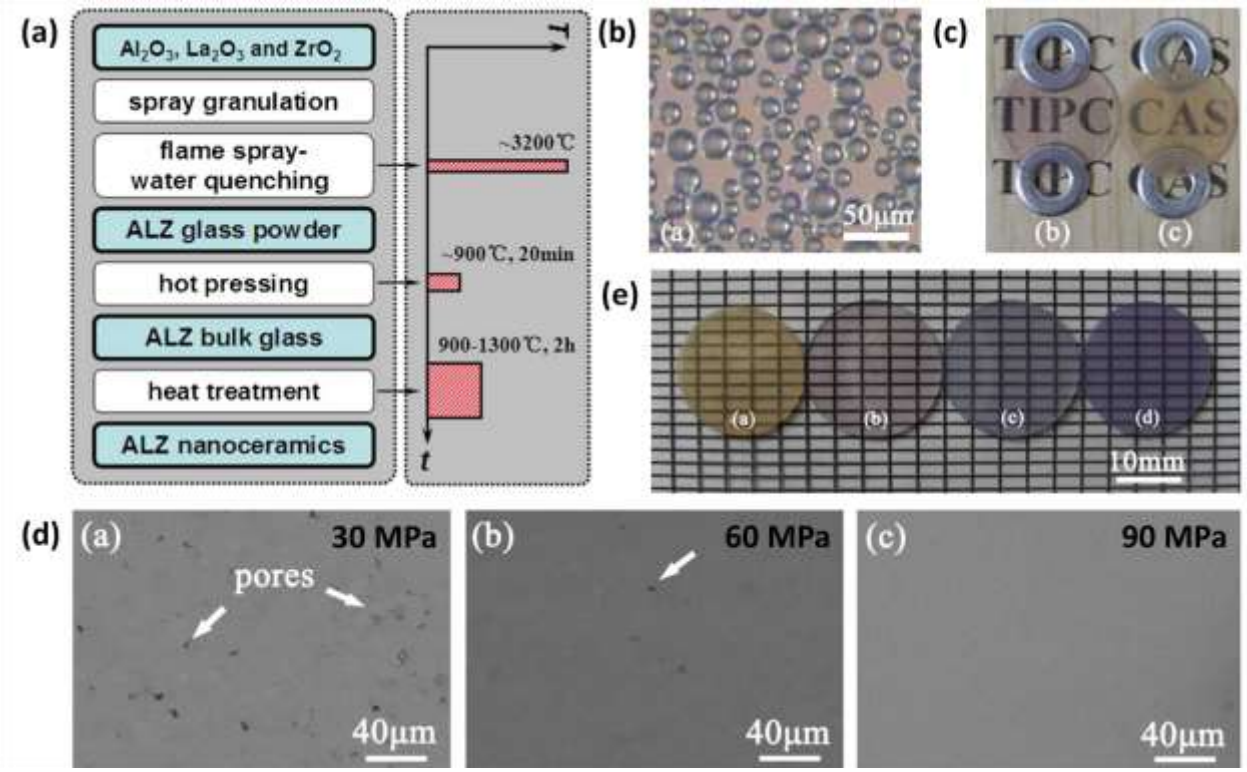

Figure 13. (a) Diagram illustrating the steps of the ASCC process; (b) Optical microscope images of $LaAlO_3/ZrO_2$ glass microspheres; (c) $LaAlO_3/ZrO_2$ glass (left) and nanoceramics (right); [146] (d) SEM images of $LaAlO_3/ZrO_2$ glass samples sintered by hot-pressing under varying pressures; (e) Transparent nanoceramics prepared via the ASCC method: (left to right) $LaAlO_3/ZrO_2$, 1.5% Er:$LaAlO_3/ZrO_2$, 1% Nd:YAG/HfO_2, and 3% Nd:YAG/HfO_2. [147]

5.5 Ultra-high pressure crystallization from glass

The application of ultra-high (GPa-range) pressure during sintering has seen investigation as a method to instigate faster nucleation while suppressing grain growth during glass crystallization, in order to form transparent ceramics with nanoscale grains. The high-pressure/low-temperature conditions are produced using a so-called multianvil apparatus, which has been successfully demonstrated as effective for the production of certain ultra-hard nanoceramics (e.g., diamond, various SiO_2 polymorphs, etc.). The approach is significantly different from performing glass crystallization in a hot-press configuration, where the applied pressure only ranges up to approximately 100 MPa. The capability to produce very small grain sizes with the ultra-high pressure method makes it ideal for producing non-cubic transparent ceramics, which suffer from high birefringence effects when grain sizes exceed a certain level. Moreover, the method also allows for metastable crystallographic phases to be produced that cannot otherwise be obtained under the intermediate pressure and high-temperature conditions observed in hot-pressing glass crystallization. These high-pressure phases are particularly of interest as they typically have higher density, hardness, elastic stiffness, etc., than low-pressure/high temperature phases.

One such demonstration of the multianvil system includes a 2016 report on $Ca_3Al_2Si_3O_{12}$ silicate garnet transparent ceramics by Irifune et al. [148] The authors first prepared a parent glass by melt-quenching of a powder mixture, which was subsequently shaped into a glass rod. The formed rod was then wrapped with a thin layer of iron foil, placed in a gold capsule, and then inserted into a specialized multianvil apparatus cell. The glass sample and containing cell were then inserted into the multianvil apparatus and subjected to ultra-high pressures (5–15 GPa) and relatively high temperatures (1100–1600^{o}C). A simplified schematic of the employed multianvil system is

depicted in **Figure 14(a)**. After preparing a set of samples at varying temperature and pressure conditions, the authors concluded that the best results were obtained by annealing at between 1300ºC and 1500ºC under an applied pressure of 15 GPa. Very small grain sizes of 30–50 nm (**Figure 14(d)**) were obtained under these conditions, which was attributed to extremely rapid nucleation but very slow grain growth. Furthermore, it was noted that reducing the applied pressure produced an increase in grain size that varied up to the micron-scale, a phenomenon speculated to be the result of nucleation rate decreasing and atomic diffusion increasing with decreasing pressure. Mechanical property characterization of the ceramics revealed an increase in hardness of approximately ~30% between the minimum and maximum grain sizes, corresponding to specimens produced at the highest and lowest pressures, respectively. Transmittance measurements of specimens annealed in the 1300–1500ºC temperature range under 15 GPa applied pressure revealed values that approached theoretical levels (**Figure 14(b)**); an observation that was attributed to the small grain size and high density/low-porosity levels of the ceramic. Importantly, the ultra-high pressure processing approach can be particularly beneficial for systems with a large mismatch between the density of the glass and crystalline phases. At ambient pressure, a large density difference can result in cracking or porosity development during the crystallization stage, whereas under ultra-high pressure conditions, a fully dense microstructure can be retained. The $Ca_3Al_2Si_3O_{12}$ garnet transparent ceramics described herein clearly illustrate this point. The effectiveness of the ultra-high pressure fabrication approach was further demonstrated by successful application of the technique to produce transparent nanoceramics of other silicate garnets, including $Ca_3Cr_2Si_3O_{12}$, $Mg_3Al_2Si_3O_{12}$, and $Mg_3Cr_2Si_3O_{12}$ (**Figure 14(c)**), often considered for application in modern jewelry production.

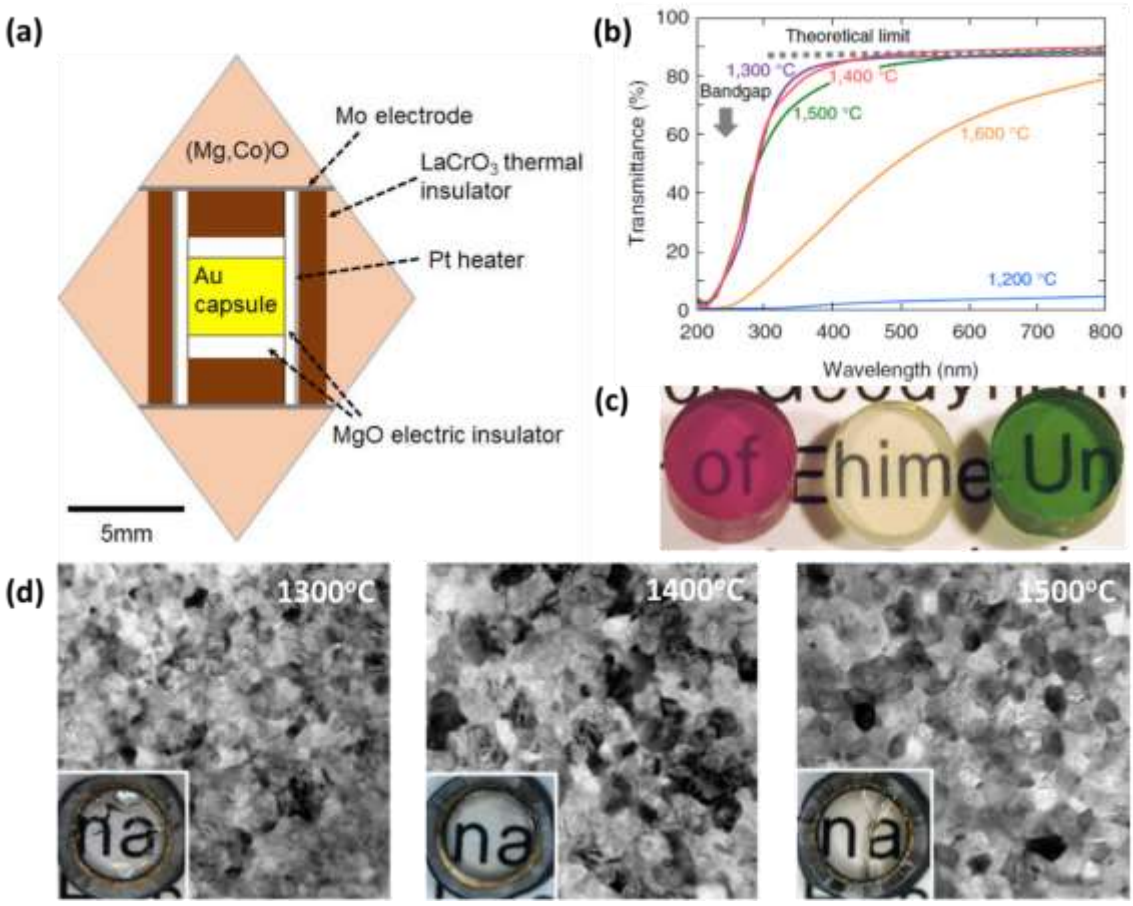

Figure 14. (a) A schematic illustration of the multianvil furnace apparatus used for the ultra-high pressure crystallization of glass; (b) Optical transmittance spectra of the $Ca_3Al_2Si_3O_{12}$ ceramic samples annealed at different temperatures; (c) Transparent $Ca_3Cr_2Si_3O_{12}$ (green), $Mg_3Al_2Si_3O_{12}$ (colorless), and $Mg_3Cr_2Si_3O_{12}$ (purple) garnet nanoceramics fabricated at 1400°C and 15 GPa applied pressure using the multianvil furnace; (d) Photographs and SEM images of $Ca_3Al_2Si_3O_{12}$ transparent ceramics samples obtained by annealing at 1300–1500°C at 15 GPa applied pressure. [148]

6. Summary and future outlook

Recent advancements in transparent ceramic fabrication technology have given transparent ceramics a number of economic and technical advantages over competing glass, glass-ceramic,

and single-crystalline materials. The range of properties that can be attained, and the ability to produce an expanded range of material compositions with flexibility in shape varieties make transparent ceramics appealing for a number of optical, optoelectronic, and other applications. However, the currently well-established methods for producing transparent ceramics rely primarily on conventional sintering methods, which suffer from drawbacks associated with obtaining acceptable grain sizes while simultaneously achieving complete densification, with the latter sometimes being difficult to achieve even with post-sintering treatments.

The glass crystallization approach has been demonstrated to be promising for circumventing these issues and allowing for highly transparent ceramics to be produced, and with new metastable phases previously unattainable by conventional techniques, such as those with anisotropic crystal structures. Although certain variations of the glass crystallization approach employ specialized equipment, such as aerodynamic levitation and multianvil systems, the approach can also be conducted with conventional ceramic processing and heat treatment equipment, making it simple and cost-effective. Fabricating a transparent ceramic from high density and very low-porosity parent glasses enables the production of polycrystalline ceramics with correspondingly low porosity; a significant advantage compared with conventional techniques in which residual porosity is a substantial source of optical losses. Additionally, the glass crystallization method has been demonstrated to be effective for producing ceramics with grain sizes in the nanoscale range, which is very challenging to achieve with conventional ceramic processing techniques, but which is critical for attaining acceptable optical properties.

Despite the positive developments with regards to the use of the glass crystallization approach to produce transparent ceramics, it should be emphasized that the method is still in the early stages of investigation, and many aspects remain relatively unknown. One significant caveat that must be

considered in establishing the overall potential of the technique, is that because the concept is a relatively new one, it is still heavily under-explored with most current knowledge originating in reports from a relatively small active community of researchers. For this reason, uncertainty still exists as to the applicability of the approach to different material systems, or whether limitations exist in terms of the chemical compositions it can be applied to. Additionally, in order for the technique to gain mainstream acceptance and see widespread application, fundamental theory, and a deeper understanding of the glass → ceramic transition and accompanying microstructural evolution must be developed. Very few studies have reflected on the theoretical background and provided an understanding of optical and transparency-related properties. The literature on the measurement of mechanical properties and related phenomena is even more scarce. Therefore, several research directions for future work may extend the current knowledge of this field and provide an in-depth understanding of various phenomena associated with the full bulk glass crystallization into transparent ceramics.

Other potential research directions may focus on the oriented crystallization of glass, an aspect particularly important to the ceramics with anisotropic structures, which would alleviate the detrimental birefringence effects on materials' transparency without the need of controlling the (nano)crystallite size. The laser-induced glass crystallization technique (laser patterning) has been efficient in creating highly oriented single-crystal-like structures along the laser scanning directions within the amorphous glass specimens; this technology could also potentially be utilized for the growth of oriented transparent ceramics from glass. Moreover, recent advancements in the 3-D printing technology of both glass and ceramic transparent materials provided strong arguments for considering this technology for the fabrication of glass crystallized ceramics with high optical qualities. However, significant leap forward in glass crystallization technique would be provided

by the development of single-crystal materials starting from the glass, as discussed in [133], which would open a door to a whole new field and unlock numerous application possibilities. However, another important point to reflect on is the potential for mass production and applicability of transparent ceramics obtained via full glass crystallization. As mentioned earlier, the first step in developing this synthesis approach is to gain a better understanding of the underlying science, which would enable better control of the process. However, the current state of technology and presented synthesis approaches allow only a lab-scale production; therefore, efforts have to be made in the future that will scale up existing or develop alternative processes to support the development of this field to gain practical and economic benefits from the production. Fortunately, the need for transparent ceramics with customizable compositions and optical properties for different applications is increasing, which is expected to stimulate and drive further development. Ultimately, however, the concept exhibits significant promise for overcoming serious and long-standing obstacles related to the fabrication of transparent ceramics, which will assuredly garner increasing research interest in coming years.

Acknowledgements

Iva Milisavljevic and Yiquan Wu gratefully acknowledge the National Science Foundation (NSF) CAREER grant (1554094) and JTO-ONR grant (N00014-17-1-2548) for funding the work.

Conflict of Interest

The authors declare no financial conflicts of interest.

References

[1] A. Goldstein, A. Krell, Z. Burshtein, Transparent Ceramics: Materials, Engineering, and Applications, John Wiley & Sons, Inc., Hoboken, NJ, USA, 2020.

[2] A. Ikesue, I. Furusato, K. Kamata, Fabrication of Polycrystalline, Transparent YAG Ceramics by a Solid-State Reaction Method, J. Am. Ceram. Soc., 78 (1995) 225-228.
[3] A. Ikesue, Y.L. Aung, Ceramic laser materials, Nat. Photonics, 2 (2008) 721-727.
[4] S.F. Wang, J. Zhang, D.W. Luo, F. Gu, D.Y. Tang, Z.L. Dong, G.E.B. Tan, W.X. Que, T.S. Zhang, S. Li, L.B. Kong, Transparent ceramics: Processing, materials and applications, Prog. Solid. State Ch., 41 (2013) 20-54.
[5] A. Ikesue, Y.L. Aung, T. Yoda, S. Nakayama, T. Kamimura, Fabrication and laser performance of polycrystal and single crystal Nd:YAG by advanced ceramic processing, Opt. Mater., 29 (2007) 1289-1294.
[6] V. Lupei, A. Lupei, A. Ikesue, Single crystal and transparent ceramic Nd-doped oxide laser materials: a comparative spectroscopic investigation, J. Alloys Compd., 380 (2004) 61-70.
[7] A. Ikesue, Polycrystalline Nd:YAG ceramics lasers, Opt. Mater., 19 (2002) 183-187.
[8] S.-J.L. Kang, J.-H. Park, S.-Y. Ko, H.-Y. Lee, Solid-State Conversion of Single Crystals: The Principle and the State-of-the-Art, J. Am. Ceram. Soc., 98 (2015) 347–360.
[9] A. Ikesue, Y.L. Aung, Synthesis and Performance of Advanced Ceramic Lasers, J. Am. Ceram. Soc., 89 (2006) 1936-1944.
[10] L. Ge, J. Li, Z. Zhou, H. Qu, M. Dong, Y. Zhu, T. Xie, W. Li, M. Chen, H. Kou, Y. Shi, Y. Pan, X. Feng, J. Guo, Fabrication of composite YAG/Nd:YAG/YAG transparent ceramics for planar waveguide laser, Opt. Mater. Express, 4 (2014) 1042-1049.
[11] Y. Shi, Q.W. Chen, J.L. Shi, Processing and scintillation properties of Eu^{3+} doped Lu_2O_3 transparent ceramics, Opt. Mater., 31 (2009) 729-733.
[12] G.H. Liu, Z.Z. Zhou, Y. Shi, Q. Liu, J.Q. Wan, Y.B. Pan, Ce:YAG transparent ceramics for applications of high power LEDs: Thickness effects and high temperature performance, Mater. Lett., 139 (2015) 480-482.
[13] G.C. Wei, Transparent ceramics for lighting, J. Eur. Ceram. Soc., 29 (2009) 237-244.
[14] U. Peuchert, Y. Okano, Y. Menke, S. Reichel, A. Ikesue, Transparent cubic-ZrO_2 ceramics for application as optical lenses, J. Eur. Ceram. Soc., 29 (2009) 283-291.
[15] H. Lin, S. Zhou, H. Teng, Synthesis of $Tb_3Al_5O_{12}$ (TAG) transparent ceramics for potential magneto-optical applications, Opt. Mater., 33 (2011) 1833-1836.
[16] A. Krell, J. Klimke, T. Hutzler, Advanced spinel and sub-µmAl_2O_3 for transparent armour applications, J. Eur. Ceram. Soc., 29 (2009) 275-281.
[17] H. Yagi, T. Yanagitani, K. Takaichi, K.-i. Ueda, A.A. Kaminskii, Characterizations and laser performances of highly transparent Nd^{3+}:$Y_3Al_5O_{12}$ laser ceramics, Opt. Mater., 29 (2007) 1258-1262.
[18] H.-L. Li, X.-J. Liu, L.-P. Huang, Fabrication of Transparent Cerium-Doped Lutetium Aluminum Garnet (LuAG:Ce) Ceramics by a Solid-State Reaction Method, J. Am. Ceram. Soc., 88 (2005) 3226-3228.
[19] J. Ueda, K. Kuroishi, S. Tanabe, Yellow persistent luminescence in Ce^{3+}–Cr^{3+}-codoped gadolinium aluminum gallium garnet transparent ceramics after blue-light excitation, Appl. Phys. Express, 7 (2014) 062201.
[20] J. Zhang, L. Ana, M. Liu, S. Shimai, S. Wang, Sintering of Yb^{3+}:Y_2O_3 transparent ceramics in hydrogen atmosphere, J. Eur. Ceram. Soc., 29 (2009) 305-309.
[21] J.-G. Li, T. Ikegami, T. Mori, Fabrication of Transparent, Sintered Sc_2O_3 Ceramics, J. Am. Ceram. Soc., 88 (2005) 817-821.

[22] D. Zhou, Y. Shi, J. Xie, Y. Ren, P. Yun, Fabrication and Luminescent Properties of Nd^{3+}-Doped Lu_2O_3 Transparent Ceramics by Pressureless Sintering, J. Am. Ceram. Soc., 92 (2009) 2182-2187.
[23] E.H. Penilla, Y. Kodera, J.E. Garay, Blue–Green Emission in Terbium-Doped Alumina (Tb:Al_2O_3) Transparent Ceramics, Adv. Funct. Mater., 23 (2013) 6036-6043.
[24] T. Kato, G. Okada, T. Yanagida, Optical, scintillation and dosimeter properties of MgO transparent ceramic doped with Mn^{2+}, J. Ceram. Soc. Jpn., 124 (2016) 559-563.
[25] L. An, A. Ito, T. Goto, Fabrication of transparent Lu_3NbO_7 by spark plasma sintering, Mater. Lett., 65 (2011) 3167-3169.
[26] C.-F. Chen, R.A. Synowicki, M.J. Brand, E.L. Tegtmeier, J.D. Montalvo, J. Ivy, G.L. Brennecka, Z. Seeley, N.J. Cherepy, S.A. Payne, Processing and characteristics of transparent Gd_3TaO_7 polycrystalline ceramics, J. Am. Ceram. Soc., 101 (2018) 1847-1856.
[27] Z.Y. Fu, J.F. Liu, H. Wang, D.H. He, Q.J. Zhang, Spark plasma sintering of aluminium nitride transparent ceramics, Mater. Sci. Technol., 20 (2004) 1097-1099.
[28] S.S. Kaplan, S. Kurama, G. Gunkaya, Spinel nitrides transparent ceramics, J. Eur. Ceram. Soc., 35 (2015) 3255-3262.
[29] F. Nakamura, T. Kato, G. Okada, N. Kawano, N. Kawaguchi, K. Fukuda, T. Yanagida, Scintillation, dosimeter and optical properties of MgF_2 transparent ceramics doped with Gd^{3+}, Mater. Res. Bull., 98 (2018) 83-88.
[30] X. Xie, B. Mei, J. Song, W. Li, L. Su, Fabrication and spectral properties of Nd, La: CaF_2 transparent ceramics, Opt. Mater., 76 (2018) 111-116.
[31] W. Li, B. Mei, J. Song, Z. Wang, Fabrication and optical property of highly transparent SrF2 ceramic, Mater. Lett., 159 (2015) 210-212.
[32] J. Li, X. Chen, L. Tang, Y. Li, Y. Wu, Fabrication and Properties of Transparent Nd-doped BaF_2 Ceramics, J. Am. Ceram. Soc., 102 (2019) 178-184.
[33] Y. Li, Y. Liu, V.V. Fedorov, S.B. Mirov, Y. Wu, Hot-pressed chromium doped zinc sulfide infrared transparent ceramics, Scr. Mater., 125 (2016) 15-18.
[34] S. Yu, D. Carloni, Y. Wu, Microstructure development and optical properties of Fe:ZnSe transparent ceramics sintered by spark plasma sintering, J. Am. Ceram. Soc., 103 (2020) 4159-4166.
[35] M. Dolhen, J. Carreaud, G. Delaizir, J.-R. Duclère, M. Vandenhende, N. Tessier-Doyen, O. Tantot, D. Passerieux, P.-E. Coulon, P. Thomas, M. Allix, S. Chenu, New $KNbTeO_6$ transparent tellurate ceramics, J. Eur. Ceram. Soc., 40 (2020) 4164-4170.
[36] K. Zhang, W. Li, J. Zeng, T. Deng, B. Luo, H. Zhang, X. Huang, Preparation of $(La_{0.2}Nd_{0.2}Sm_{0.2}Gd_{0.2}Yb_{0.2})_2Zr_2O_7$ high-entropy transparent ceramic using combustion synthesized nanopowder, J. Alloys Compd., 817 (2020) 153328.
[37] X. Chen, Y. Wu, High-entropy transparent fluoride laser ceramics, J. Am. Ceram. Soc., 103 (2019) 750-756.
[38] Y. Sato, J. Akiyama, T. Taira, Orientation control of micro-domains in anisotropic laser ceramics, Opt. Mater. Express, 3 (2013) 829-841.
[39] H. Furuse, N. Horiuchi, B.-N. Kim, Transparent non-cubic laser ceramics with fine microstructure, Sci. Rep., 9 (2019) 10300.
[40] S. Chen, Y. Wu, Y. Yang, Spark Plasma Sintering of Hexagonal Structure Yb^{3+}-Doped $Sr_5(PO_4)_3F$ Transparent Ceramics, J. Am. Ceram. Soc., 96 (2013) 1694-1697.
[41] Z. Wei, Y. Huang, T. Tsuboi, Y. Nakai, J. Zeng, G. Li, Optical characteristics of Er^{3+}-doped PMN–PT transparent ceramics, Ceram. Int., 38 (2012) 3397-3402.

[42] W. Ruan, G. Li, J. Zeng, J. Bian, L.S. Kamzina, H. Zeng, L. Zheng, A. Ding, Large Electro-Optic Effect in La-Doped 0.75Pb($Mg_{1/3}Nb_{2/3}$)O_3–0.25$PbTiO_3$ Transparent Ceramic by Two-Stage Sintering, J. Am. Ceram. Soc., 93 (2010) 2128-2131.
[43] A.S.S.d. Camargo, J.F. Possatto, L.A.d.O. Nunes, E.R. Botero, E.R.M. Andreeta, D. Garcia, J.A. Eiras, Infrared to visible frequency upconversion temperature sensor based on Er^{3+}-doped PLZT transparent ceramics, Solid State Commun., 137 (2006) 1-5.
[44] Z. Xiao, S. Yu, Y. Li, S. Ruan, L.B. Kong, Q. Huang, Z. Huang, K. Zhou, H. Su, Z. Yao, W. Que, Y. Liu, T. Zhang, J. Wang, P. Liu, D. Shen, M. Allix, J. Zhang, D. Tang, Materials development and potential applications of transparent ceramics: A review, Mater. Sci. Eng. R, 139 (2020) 100518.
[45] C. Chlique, O. Merdrignac-Conanec, N. Hakmeh, X. Zhang, J.-L. Adam, Transparent ZnS Ceramics by Sintering of High Purity Monodisperse Nanopowders, J. Am. Ceram. Soc., 96 (2013) 3070-3074.
[46] G.R. Durand, Q. Bizot, N. Herbert, S. Quéméré, M. Pasturel, X.-H. Zhang, O. Merdrignac-Conanec, Processing of $CaLa_2S_4$ infrared transparent ceramics: A comparative study of HP and FAST/SPS techniques, J. Am. Ceram. Soc., 103 (2020).
[47] L. Calvez, Chalcogenide glasses and glass-ceramics: Transparent materials in the infrared for dual applications, C. R. Physique, 18 (2017) 314-322.
[48] K.A. Richardson, M. Kang, L. Sisken, A. Yadav, S. Novak, A. Lepicard, I. Martin, H. Francois-Saint-Cyr, C.M. Schwarz, T.S. Mayer, C. Rivero-Baleine, A.J. Yee, I. Mingareev, Advances in infrared gradient refractive index (GRIN) materials: a review, Opt. Eng., 59 (2020) 112602.
[49] M. Hubert, G. Delaizir, J. Monnier, C. Godart, H.-L. Ma, X.-H. Zhang, L. Calvez, An innovative approach to develop highly performant chalcogenide glasses and glass-ceramics transparent in the infrared range, Opt. Express, 19 (2011) 23513.
[50] B. Xue, L. Calvez, M. Allix, G. Delaizir, X.-H. Zhang, Amorphization by Mechanical Milling for Making IR Transparent Glass-Ceramics, J. Am. Ceram. Soc., 99 (2016) 1573-1578.
[51] M. Wakaki, Optical Materials and Applications, CRC Press, Boca Ranton, FL, USA, 2017.
[52] O. Stenzel, Light–Matter Interaction, Springer Nature, Cham, Switzerland, 2022.
[53] J.H. Simmons, K.S. Potter, Optical Materials, Academic Press, San Diego, CA, USA, 2000.
[54] W. Pabst, J. Hostaša, L. Esposito, Porosity and pore size dependence of the real in-line transmission of YAG and alumina ceramics, J. Eur. Ceram. Soc., 34 (2014) 2745-2756.
[55] N.T. Hieu, D.V. Thom, A new experimental approach to measure the refractive index of infrared optical ceramic through the transmittance, Ceram. Int., 46 (2020) 25726-25730.
[56] R. Apetz, M.P.B.v. Bruggen, Transparent Alumina: A Light-Scattering Model, J. Am. Ceram. Soc., 86 (2003) 480-486.
[57] S.J. Dillon, M.P. Harmer, Relating Grain-Boundary Complexion to Grain-Boundary Kinetics I: Calcia-Doped Alumina, J. Am. Ceram. Soc., 91 (2008) 2304–2313.
[58] B.-N. Kim, K. Hiraga, K. Morita, H. Yoshida, Spark plasma sintering of transparent alumina, Scr. Mater., 57 (2007) 607-610.
[59] B.-N. Kim, K. Morita, N. Horiuchi, H. Yoshida, A. Dash, J.-G. Li, Y.-W. Kim, Y. Sakka, Spark Plasma Sintering of Highly Transparent Hydroxyapatite Ceramics, J. Jpn. Soc. Powder Powder Metall., 64 (2017) 547-551.
[60] J. Akiyama, Y. Sato, T. Taira, Laser Demonstration of Diode-Pumped Nd^{3+}-Doped Fluorapatite Anisotropic Ceramics, Appl. Phys. Express, 4 (2011) 022703.

[61] B.-N. Kim, K. Hiraga, K. Morita, H. Yoshida, T. Miyazaki, Y. Kagawa, Microstructure and optical properties of transparent alumina, Acta Mater., 57 (2009) 1319-1326.
[62] S.-H. Lee, S. Kochawattana, G.L. Messing, J.Q. Dumm, G. Quarles, V. Castillo, Solid-State Reactive Sintering of Transparent Polycrystalline Nd:YAG Ceramics, J. Am. Ceram. Soc., 89 (2006) 1945-1950.
[63] J. Xu, Y. Shi, J. Xie, F. Lei, Fabrication, Microstructure, and Luminescent Properties of Ce^{3+}-Doped $Lu_3Al_5O_{12}$ (Ce:LuAG) Transparent Ceramics by Low-Temperature Vacuum Sintering, J. Am. Ceram. Soc., 96 (2013) 1930-1936.
[64] L. Zhang, W. Pan, Structural and Thermo-Mechanical Properties of Nd: Y_2O_3 Transparent Ceramics, J. Am. Ceram. Soc., 98 (2015) 3326-3331.
[65] Y. Huang, D. Jiang, J. Zhang, Q. Lin, Z. Huang, Sintering of Transparent Yttria Ceramics in Oxygen Atmosphere, J. Am. Ceram. Soc., 93 (2010) 2964-2967.
[66] J. Wang, J. Ma, J. Zhang, P. Liu, D. Luo, D. Yin, D. Tang, L.B. Kong, Yb:Y_2O_3 transparent ceramics processed with hot isostatic pressing, Opt. Mater., 71 (2017) 117-120.
[67] W. Zhang, T. Lu, B. Ma, N. Wei, Z. Lu, F. Li, Y. Guan, X. Chen, W. Liu, L. Qi, Improvement of optical properties of Nd:YAG transparent ceramics by post-annealing and post hot isostatic pressing, Opt. Mater., 35 (2013) 2405-2410.
[68] K. Itatani, T. Tsujimoto, A. Kishimoto, Thermal and optical properties of transparent magnesium oxide ceramics fabricated by post hot-isostatic pressing, J. Eur. Ceram. Soc., 26 (2006) 639-645.
[69] K. Tsukuma, I. Yamashita, T. Kusunose, Transparent 8 mol% Y_2O_3–ZrO_2 (8Y) Ceramics, J. Am. Ceram. Soc., 91 (2008) 813-818.
[70] Z.M. Seeley, N.J. Cherepy, S.A. Payne, Homogeneity of Gd-based garnet transparent ceramic scintillators for gamma spectroscopy, J. Cryst. Growth, 379 (2013) 79-83.
[71] L. Jin, G. Zhou, S. Shimai, J. Zhang, S. Wang, ZrO_2-doped Y_2O_3 transparent ceramics via slip casting and vacuum sintering, J. Eur. Ceram. Soc., 30 (2010) 2139-2143.
[72] X. Ba, J. Li, Y. Pan, Y. Zeng, H. Kou, W. Liu, J. Liu, L. Wu, J. Guo, Comparison of aqueous- and non-aqueous-based tape casting for preparing YAG transparent ceramics, J. Alloys Compd., 577 (2013) 228-231.
[73] I.K. Jones, Z.M. Seeley, N.J. Cherepy, E.B. Duoss, S.A. Payne, Direct ink write fabrication of transparent ceramic gain media, Opt. Mater., 75 (2018) 19-25.
[74] W.K. Jung, H.J. Ma, H.-N. Kim, D.K. Kim, Transparent Ceramics for Visible/IR Windows: Processing, Materials and Characterization, Korean J. Mater. Res., 28 (2018) 551-563.
[75] L. Esposito, A. Piancastelli, S. Martelli, Production and characterization of transparent $MgAl_2O_4$ prepared by hot pressing, J. Eur. Ceram. Soc., 33 (2013) 737-747.
[76] J. Liu, P. Liu, J. Wang, X. Xu, D. Li, J. Zhang, X. Nie, Fabrication and Sintering Behavior of Er:SrF_2 Transparent Ceramics using Chemically Derived Powder, Materials, 11 (2018) 475.
[77] S.S. Balabanov, R.P. Yavetskiy, A.V. Belyaev, E.M. Gavrishchuk, V.V. Drobotenko, I.I. Evdokimov, A.V. Novikova, O.V. Palashov, D.A. Permin, V.G. Pimenov, Fabrication of transparent $MgAl_2O_4$ ceramics by hot-pressing of sol-gel-derived nanopowders, Ceram. Int., 41 (2015) 13366-13371.
[78] J. Zhang, T. Lu, X. Chang, N. Wei, W. Xu, Related mechanism of transparency in $MgAl_2O_4$ nano-ceramics prepared by sintering under high pressure and low temperature, J. Phys. D: Appl. Phys., 42 (2009) 052002.

[79] S.R. Podowitz, R. Gaume, R.S. Feigelson, Effect of Europium Concentration on Densification of Transparent Eu:Y_2O_3 Scintillator Ceramics Using Hot Pressing, J. Am. Ceram. Soc., 93 (2010) 82-88.
[80] Z. Geng, K. Li, X. Li, D. Shi, Fabrication and photoluminescence of Eu-doped KNN-based transparent ceramics, J. Mater. Sci., 52 (2017) 2285-2295.
[81] K. Liu, D. He, H. Wang, T. Lu, F. Li, X. Zhou, High-pressure sintering mechanism of yttrium aluminum garnet ($Y_3Al_5O_{12}$) transparent nanoceramics, Scr. Mater., 66 (2012) 319-322.
[82] K. Morita, B.-N. Kim, K. Hiraga, H. Yoshida, Fabrication of transparent $MgAl_2O_4$ spinel polycrystal by spark plasma sintering processing, Scr. Mater., 58 (2008) 1114-1117.
[83] C. Mével, J. Carreaud, G. Delaizir, J.-R. Duclére, F. Brisset, J. Bourret, P. Carles, C. Genevois, M. Allix, S. Chenu, First $ZnGa_2O_4$ transparent ceramics, J. Eur. Ceram. Soc., 41 (2021) 4934-4941.
[84] G. Bonnefont, G. Fantozzi, S. Trombert, L. Bonneau, Fine-grained transparent $MgAl_2O_4$ spinel obtained by spark plasma sintering of commercially available nanopowders, Ceram. Int., 38 (2012) 131-140.
[85] B.-N. Kim, K. Hiraga, A. Jeong, C. Hu, T.S. Suzuki, J.-D. Yun, Y. Sakka, Transparent $ZnAl_2O_4$ ceramics fabricated by spark plasma sintering, J. Ceram. Soc. Jpn., 122 (2014) 784-787.
[86] Y. Futami, T. Yanagida, Y. Fujimoto, J. Pejchal, M. Sugiyama, S. Kurosawa, Y. Yokota, A. Ito, A. Yoshikawa, T. Goto, Optical and scintillation properties of Sc_2O_3,Y_2O_3 and Lu_2O_3 transparent ceramics synthesized by SPS method, Radiat. Meas., 55 (2013) 136-140.
[87] R. Chaim, M. Kalina, J.Z. Shen, Transparent yttrium aluminum garnet (YAG) ceramics by spark plasma sintering, J. Eur. Ceram. Soc., 27 (2007) 3331-3337.
[88] G. Zhang, D. Carloni, Y. Wu, Ultraviolet emission transparent Gd:YAG ceramics processed by solid-state reaction spark plasma sintering, J. Am. Ceram. Soc., 103 (2020) 839-848.
[89] S. Grasso, H. Yoshida, H. Porwal, Y. Sakka, M. Reece, Highly transparent α-alumina obtained by low cost high pressure SPS, Ceram. Int., 39 (2013) 3243-3248.
[90] H.B. Zhang, B.-N. Kima, K. Morita, H. Yoshida, J.-H. Lim, K. Hiraga, Optimization of high-pressure sintering of transparent zirconia with nano-sized grains, J. Alloys Compd., 508 (2010) 196-199.
[91] N. Jiang, R.-j. Xie, Q. Liu, J. Li, Fabrication of sub-micrometer MgO transparent ceramics by spark plasma sintering, J. Eur. Ceram. Soc., 37 (2017) 4947-4953.
[92] P. Wang, M. Yang, S. Zhang, R. Tu, T. Goto, L. Zhang, Suppression of carbon contamination in SPSed CaF_2 transparent ceramics by Mo foil, J. Eur. Ceram. Soc., 37 (2017) 4103-4107.
[93] Y. Chen, L. Zhang, J. Zhang, P. Liu, T. Zhou, H. Zhang, D. Gong, D. Tang, D. Shen, Fabrication of transparent ZnS ceramic by optimizing the heating rate in spark plasma sintering process, Opt. Mater., 50 (2015) 36-39.
[94] J. Luo, H. Tu, L. Deng, Z. Zhong, Preparation of Zirconia Transparent Ceramics by Low Temperature Microwave Sintering, J. Nanosci. Nanotechnol., 14 (2014) 3965-3968.
[95] G. Kerbart, C. Harnois, C. Bilot, S. Marinel, Pressure-assisted microwave sintering: A rapid process to sinter submicron sized grained $MgAl_2O_4$ transparent ceramics, J. Eur. Ceram. Soc., 39 (2019) 2946-2951.
[96] M.N. Rahaman, Ceramic Processing and Sintering, CRC Press, Boca Raton, Florida, USA, 2017.
[97] E. Véron, M.N. Garaga, D. Pelloquin, S. Cadars, M. Suchomel, E. Suard, D. Massiot, V. Montouillout, G. Matzen, M. Allix, Synthesis and Structure Determination of $CaSi_{1/3}B_{2/3}O_{8/3}$: A New Calcium Borosilicate, Inorg. Chem., 52 (2013) 4250-4258.

[98] A. Rosenflanz, M. Frey, B. Endres, T. Anderson, E. Richards, C. Schardt, Bulk glasses and ultrahard nanoceramics based on alumina and rare-earth oxides, Nature, 430 (2004) 761-764.
[99] M. Allix, S. Alahrache, F. Fayon, M. Suchomel, F. Porcher, T. Cardinal, G. Matzen, Highly Transparent $BaAl_4O_7$ Polycrystalline Ceramic Obtained by Full Crystallization from Glass, Adv. Mater., 24 (2012) 5570-5575.
[100] S. Alahraché, K.A. Saghir, S. Chenu, E. Véron, D.D.S. Meneses, A.I. Becerro, M. Ocaña, F. Moretti, G. Patton, C. Dujardin, F. Cussó, J.-P. Guin, M. Nivard, J.-C. Sangleboeuf, G. Matzen, M. Allix, Perfectly Transparent $Sr_3Al_2O_6$ Polycrystalline Ceramic Elaborated from Glass Crystallization, Chem. Mater., 25 (2013) 4017-4024.
[101] A. Bertrand, J. Carreaud, S. Chenu, M. Allix, E. Véron, J.-R. Duclère, Y. Launay, T. Hayakawa, C. Genevois, F. Brisset, F. Célarié, P. Thomas, G. Delaizir, Scalable and Formable Tellurite-Based Transparent Ceramics for Near Infrared Applications, Adv. Opt. Mater., 4 (2016) 1482-1486.
[102] J. Deubener, M. Allix, M.J. Davis, A. Duran, T. Höche, T. Honma, T. Komatsu, S. Krüger, I. Mitra, R. Müller, S. Nakane, M.J. Pascual, J.W.P. Schmelzer, E.D. Zanotto, S. Zhou, Updated definition of glass-ceramics, J. Non-Cryst. Solids, 501 (2018) 3-10.
[103] Z. Fang, R. Cao, F. Zhang, Z. Ma, G. Dong, J. Qiu, Efficient spectral conversion from visible to nearinfrared in transparent glass ceramics containing Ce^{3+}–Yb^{3+} codoped $Y_3Al_5O_{12}$ nanocrystals, J. Mater. Chem. C, 2 (2014) 2204-2211.
[104] P.A. Loiko, O.S. Dymshits, I.P. Alekseeva, A.A. Zhilin, M.Y. Tsenter, E.V. Vilejshikova, K.V. Bogdanov, X. Mateos, K.V. Yumashev, Transparent glass–ceramics with (Eu^{3+},Yb^{3+}):$YNbO_4$ nanocrystals: Crystallization, structure, optical spectroscopy and cooperative upconversion, J. Lumin., 179 (2016) 64-73.
[105] C. Bocker, C. Russel, I. Avramov, Transparent Nano Crystalline Glass-Ceramics by Interface Controlled Crystallization, Int. J. Appl. Glass Sci., 4 (2013) 174-181.
[106] T. Berthier, V.M. Fokin, E.D. Zanotto, New large grain, highly crystalline, transparent glass–ceramics, J. Non-Cryst. Solids, 354 (2008) 1721-1730.
[107] X. Liu, J. Zhou, S. Zhou, Y. Yue, J. Qiu, Transparent glass-ceramics functionalized by dispersed crystals, Prog. Mater. Sci., 97 (2018) 38-96.
[108] G.H. Beall, D.A. Duke, Transparent Glass-Ceramics, J. Mater. Sci., 4 (1969) 340-352.
[109] G.H. Beall, L.R. Pinckney, Nanophase Glass-Ceramics, J. Am. Ceram. Soc., 82 (1999) 5-16.
[110] M.C. Gonçalves, L.F. Santos, R.M. Almeida, Rare-earth-doped transparent glass ceramics, C. R. Chimie, 5 (2002) 845-854.
[111] Y. Yamazaki, Y. Takahashi, R. Ihara, T. Fujiwara, Surface crystallization of Fresnoite-type crystallized glasses with large thickness, J. Ceram. Soc. Jpn., 119 (2011) 757-762.
[112] Y. Fujimoto, Y. Benino, T. Fujiwara, R. Sato, T. Komatsu, Transparent Surface and Bulk Crystallized Glasses with Lanthanide Tellurite Nanocrystals, J. Ceram. Soc. Jpn., 109 (2001) 466-469.
[113] E.D. Zanotto, J.C. Mauro, The glassy state of matter: Its definition and ultimate fate, J. Non-Cryst. Solids, 471 (2017) 490-495.
[114] Y. Li, S. Zhou, H. Lin, X. Hou, W. Li, H. Teng, T. Jia, Fabrication of Nd:YAG transparent ceramics with TEOS, MgO and compound additives as sintering aids, J. Alloys Compd., 502 (2010) 225-230.
[115] S. Wen, Y. Wang, B. Lan, W. Zhang, Z. Shi, S. Lv, Y. Zhao, J. Qiu, S. Zhou, Pressureless Crystallization of Glass for Transparent Nanoceramics, Adv. Sci., (2019) 1901096.

[116] K.A. Saghir, S. Chenu, E. Veron, F. Fayon, M. Suchomel, C. Genevois, F. Porcher, G. Matzen, D. Massiot, M. Allix, Transparency through Structural Disorder: A New Concept for Innovative Transparent Ceramics, Chem. Mater., 27 (2015) 508-514.
[117] M. Boyer, S. Alahraché, C. Genevois, M. Licheron, F.-X. Lefevre, C. Castro, G. Bonnefont, G. Patton, F. Moretti, C. Dujardin, G. Matzen, M. Allix, Enhanced Transparency through Second Phase Crystallization in $BaAl_4O_7$ Scintillating Ceramics, Cryst. Growth Des., 16 (2016) 386-395.
[118] W. Höland, G.H. Beall, Glass-ceramic technology, ohn Wiley & Sons, Inc., Hoboken, NJ, USA, 2012.
[119] D.R. Neuville, L. Cormier, D. Caurant, L. Montagne, From glass to crystal: Nucleation, growth and phase separation: from research to applications, EDP Sciences, Les Ulis, France, 2017.
[120] J.D. Musgraves, J. Hu, L. Calvez, Springer Handbook of Glass, Springer Nature Switzerland AG, Cham, Switzerland, 2019.
[121] A.d. Pablos-Martin, A. Duran, M.J. Pascual, Nanocrystallisation in oxyfluoride systems: mechanisms of crystallisation and photonic properties, Int. Mater. Rev., 57 (2012) 165-186.
[122] S. Chenu, E. Véron, C. Genevois, G. Matzen, T. Cardinal, A. Etienne, D. Massiot, M. Allix, Tuneable Nanostructuring of Highly Transparent Zinc Gallogermanate Glasses and Glass-Ceramics, Adv. Optical Mater., 2 (2014) 364-372.
[123] S. Araki, M. Yoshimura, Transparent Nano-Composites Ceramics by Annealing of Amorphous Phase in the HfO_2-Al_2O_3-$GdAlO_3$ System, Int. J. Appl. Ceram. Technol., 1 (2004) 155-160.
[124] S. Araki, M. Yoshimura, Fabrication of transparent ceramics through melt solidification of near eutectic compositions in HfO_2–Al_2O_3–$GdAlO_3$ system, J. Eur. Ceram. Soc., 26 (2006) 3295-3299.
[125] J.K.R. Weber, J.G. Abadie, A.D. Hixson, P.C. Nordine, G.A. Jerman, Glass Formation and Polyamorphism in Rare-Earth Oxide–Aluminum Oxide Compositions, J. Am. Ceram. Soc., 83 (2000) 1868-1872.
[126] D.A. Winborne, P.C. Nordine, D.E. Rosner, N.F. Marley, Aerodynamic Levitation Technique for Containerless High Temperature Studies on Liquid and Solid Samples, Metall. Trans. B, 7B (1976) 711-713.
[127] M. Boyer, A.J.F. Carrion, S. Ory, A.I. Becerro, S. Villette, S.V. Eliseeva, S. Petoud, P. Aballea, G. Matzena, M. Allix, Transparent polycrystalline $SrREGa_3O_7$ melilite ceramics: potential phosphors for tuneable solid state lighting, J. Mater. Chem. C, 4 (2016) 3238-3247.
[128] G. Patton, F. Moretti, A. Belsky, K.A. Saghir, S. Chenu, G. Matzen, M. Allix, C. Dujardin, Light yield sensitization by X-ray irradiation in $BaAl_4O_7 : Eu^{2+}$ ceramic scintillator obtained by full crystallization from glass, Phys. Chem. Chem. Phys., 16 (2014) 24824-24829.
[129] M. Boyer, X. Yang, A.J.F. Carrion, Q. Wang, E. Véron, C. Genevois, L. Hennet, G. Matzen, E. Suard, D. Thiaudière, C. Castro, D. Pelloquin, L.B. Kong, X. Kuang, M. Allix, First Transparent Oxide Ionic Conducting Ceramics Synthesized by Full Crystallization from Glass, J. Mater. Chem. A, 6 (2018) 5276-5289.
[130] C. Genevois, H. Bazzaoui, M. Boyer, S. Ory, Y. Ledemi, Y. Messaddeq, M.J. Pitcher, M. Allix, Emergence of A-Site Cation Order in the Small Rare-Earth Melilites Sr*RE*Ga_3O_7 (*RE* =Dy−Lu, Y), Inorg. Chem., 60 (2021) 12339-12354.
[131] J. Xu, J. Wang, A. Rakhmatullin, S. Ory, A.J. Fernandez-Carrion, H. Yi, X. Kuang, M. Allix, Interstitial Oxide Ion Migration Mechanism in Aluminate Melilite $La_{1+x}Ca_{1-x}Al_3O_{7+0.5x}$ Ceramics Synthesized by Glass Crystallization, ACS Appl. Energy Mater., 2 (2019) 2878-2888.

[132] J. Fan, V. Sarou-Kanian, X. Yang, M. Diaz-Lopez, F. Fayon, X. Kuang, M.J. Pitcher, M. Allix, $La_2Ga_3O_{7.5}$: A Metastable Ternary Melilite with a Super-Excess of Interstitial Oxide Ions Synthesized by Direct Crystallization of the Melt, Chem. Mater., 32 (2020) 9016-9025.
[133] W. Wisniewski, M.J. Pitcher, E. Veron, J. Fan, V. Sarou-Kanian, F. Fayon, M. Allix, Macroscopic Orientation Domains Grown via Aerodynamic Levitation: A Path toward Single Crystals, Cryst. Growth Des., 21 (2021) 3554-3561.
[134] A.J.F. Carrion, K.A. Saghir, E. Veron, A.I. Becerro, F. Porcher, W. Wisniewski, G. Matzen, F. Fayon, M. Allix, Local Disorder and Tunable Luminescence in $Sr_{1-x/2}Al_{2-x}Si_xO_4$ ($0.2 \leq x \leq 0.5$) Transparent Ceramics, Inorg. Chem., 56 (2017) 14446-14458.
[135] W. Wisniewski, A.J.F. Carrion, P. Schoppe, C. Rüssel, M. Allix, Oriented nucleation and crystal growth in $SrO–Al_2O_3–SiO_2$ tectosilicate glasses, CrystEngComm, 20 (2018) 3455-3466.
[136] V. Castaing, C. Monteiro, A.D. Sontakke, K. Asami, J. Xu, A.J.F. Carrión, M.G. Brik, S. Tanabe, M. Allix, B. Viana, Hexagonal $Sr_{1-x/2}Al_{2-x}Si_xO_4:Eu^{2+},Dy^{3+}$ transparent ceramics with tuneable persistent luminescence properties, Dalton Trans., 49 (2020) 16849-16859.
[137] X. Ma, X. Li, J. Li, C. Genevois, B. Ma, A. Etienne, C. Wan, E. Véron, Z. Peng, M. Allix, Pressureless glass crystallization of transparent yttrium aluminum garnet-based nanoceramics, Nat. Commun., 9 (2018) 1175.
[138] Y. Zhang, X. Ma, X. Li, L. Yang, B. Ge, M. Allix, J. Li, Crystallization kinetics of Al_2O_3-26mol%Y_2O_3 glass and full crystallized transparent $Y_3Al_5O_{12}$-based nanoceramic, J. Eur. Ceram. Soc., 41 (2021) 1557-1563.
[139] J. Han, Z. Wang, J. Li, X. Li, J. Li, G. He, J. Xie, Large-sized La_2O_3-TiO_2 high refractive glasses with low SiO_2 fraction by hot-press sintering, Int. J. Appl. Glass. Sci., 10 (2019) 371-377.
[140] L. Renyi, L. Jianqiang, L. Xiaoyu, M. Xiaoguang, L. Yanguo, S. Ming, L. Jiangtao, H. Gang, Z. Jianling, Preparation of the Large-sized La_2O_3-Nb_2O_5 Amorphous Oxide by Containerless Solidification-superplastic Hot-press Sintering, Rare Met. Mater. Eng., 47 (2018) 231-235.
[141] Z. Wang, J.-J. Han, J.-Q. Li, X.-Y. Li, J.-T. Li, G. He, J. Xie, Plastic Sintering Behavior of Large-sized La_2O_3-TiO_2-ZrO_2 Amorphous Bulk, J. Inorg. Mater., 34 (2019) 433-438.
[142] M. Dolhen, M. Tanaka, V. Couderc, S. Chenu, G. Delaizir, T. Hayakawa, J. Cornette, F. Brisset, M. Colas, P. Thomas, J.-R. Duclère, Nd^{3+}-doped transparent tellurite ceramics bulk lasers, Sci. Rep., 8 (2018) 4640.
[143] M. Dolhen, M. Allix, V. Sarou-Kanian, F. Fayon, C. Genevois, S. Chenu, P.-E. Coulon, M. Colas, J. Cornette, J.-R. Duclère, F. Brisset, O. Masson, P. Thomas, G. Delaizir, A comprehensive study of the glass / translucent anti-glass / transparent ceramic structural ordering in the Bi_2O_3-Nb_2O_5-TeO_2 system, Acta Mater., 189 (2020) 73-84.
[144] Y. Qiang, Z. Pan, M. Liang, J. Xu, X. Ye, L. Xia, W. You, J. Fu, H. Ming, Highly transparent and color-adjustable Eu^{2+} doped SrO-SiO_2-Al_2O_3 multilayered glass ceramic prepared by controlling crystallization from glass, J. Eur. Ceram. Soc., 39 (2019) 3856-3866.
[145] J. Tang, S. Lv, Z. Lin, G. Du, M. Tang, X. Feng, J. Guo, X. Li, J. Chen, L. Wei, J. Qiu, S. Zhou, Pressureless crystallization of glass toward scintillating composite with high crystallinity for radiation detection, J. Mater. Sci. Technol., 129 (2022) 173-180.
[146] L. Mei, G. He, L.-L. Wang, G.-H. Liu, J.-T. Li, Fabrication of transparent $LaAlO_3$/t-ZrO_2 nanoceramics through controlled amorphous crystallization, J. Eur. Ceram. Soc., 31 (2011) 1603-1609.
[147] L. Mei, G.-H. Liu, G. He, L.-L. Wang, J.-T. Li, Controlled amorphous crystallization: An easy way to make transparent nanoceramics, Opt. Mater., 34 (2012) 981-985.

[148] T. Irifune, K. Kawakami, T. Arimoto, H. Ohfuji, T. Kunimoto, T. Shinme, Pressure-induced nano-crystallization of silicate garnets from glass, Nat. Commun., 7 (2016) 13753.

List of figure captions

Figure 1. Schematic illustrating an optical path of light traversing transparent ceramics. [55]

Figure 2. Schematic illustration showing the in-line transmittance measurement of ceramics with refractive index n_1, exhibiting scattering from the light-scattering centers with an n_2 index of refraction. [1]

Figure 3. Schematic of the grain size effect on Mie scattering in non-cubic ceramics with grains (a) larger than and (b) comparable to or smaller (Rayleigh scattering) than the wavelength of incident light, and consequent effects on the amount of transmitted light. [39]

Figure 4. (a) SEM micrograph of YAG transparent ceramics fabricated via pressureless vacuum sintering at 1800°C for 16 h; [62] (b) EBSD map of $ZnGa_2O_4$ transparent ceramics with grain size distribution chart in the inset; (c) TEM micrograph showing porosity at the grain triple junction, and (d) high-resolution TEM image of the thin grain boundary in Cr^{3+}-doped $ZnGa_2O_4$ transparent ceramics. [83]

Figure 5. (a), (b), (e) Photographs and (c), (f) TEM micrographs of HfO_2–Al_2O_3–$GdAlO_3$ samples annealed at different temperatures and times; (d) Optical transmission spectra of the parent glass and annealed ceramic samples. [123]

Figure 6. Schematic representing aerodynamic levitation (ADL) system. [99]

Figure 7. (a) Model crystal structures of α-$BaAl_4O_7$ and β-$BaAl_4O_7$ polymorphs and (b) photograph and optical transmittances of the $BaAl_4O_7$ parent glass and corresponding ceramics; [99] (c) TEM micrograph of the $BaAl_4O_7$ ceramic matrix with dispersed $BaAl_2O_4$ nano-sized crystallites and (d) schematic depicting the proposed crystallization mechanism in the $BaAl_4O_7$–$BaAl_2O_4$ biphasic transparent ceramics. [117]

Figure 8. Inverse pole figures (IPF) of the EBSD scans of $Sr_{1-x/2}Al_{2-x}Si_xO_4$ glasses with Sr content of (a) 0.55, (b) 0.65, and (c) 0.75, displaying the changes in the crystal growth directions between the surface and bulk. [135]

Figure 9. (a) Transmission spectrum and photograph, and (b) high-resolution TEM micrograph confirming the co-existence of two crystalline phases (YAG and Al_2O_3) in YAG–Al_2O_3 transparent ceramics obtained by full crystallization from the glass phase. [137]

Figure 10. (a) Photograph and optical transmittance spectrum, (b) high-resolution TEM micrograph taken at the interface between grains (red arrows emphasize the location of the thin grain boundary), and (c) SEM micrograph depicting the crystal growth oriented perpendicularly to the surface of $Sr_{1+x/2}Al_{2+x}Si_{2-x}O_8$ (x = 0.2) transparent ceramics. [116]

Figure 11. (a) Photograph and optical transmittance spectra of transparent Nd^{3+}-doped $Bi_{0.8}Nb_{0.8}Te_{2.4}O_8$ tellurite ceramics obtained by annealing at 510°C for 5 min and 15 min; [142] (b) EBSD images of anti-glass and two transparent ceramic samples of $Bi_{0.8}Nb_{0.8}Te_{2.4}O_8$ composition, obtained via the melt-quenching method; TEM and high-resolution TEM micrographs of (c) anti-glass and (d) ceramic samples in (b). [143]

Figure 12. (a) Schematic suggesting the adjustments in the nucleation (I) vs. growth (V) rate curves for suppressing (top) or enhancing (bottom) the nucleation process; (b) and (c) SEM images of $Bi_{0.8}Nb_{0.8}Te_{2.4}O_8$ microceramics and nanoceramics, respectively, obtained on the basis of the models in (a). Optical transmission spectra and photographs of $Bi_{0.8}Nb_{0.8}Te_{2.4}O_8$ tellurite ceramics with (d) micron-scale and (e) nanometer-scale grains. [115]

Figure 13. (a) Diagram illustrating the steps of the ASCC process; (b) Optical microscope images of $LaAlO_3/ZrO_2$ glass microspheres; (c) $LaAlO_3/ZrO_2$ glass (left) and nanoceramics (right); [146] (d) SEM images of $LaAlO_3/ZrO_2$ glass samples sintered by hot-pressing under varying pressures;

(e) Transparent nanoceramics prepared via the ASCC method: (left to right) $LaAlO_3/ZrO_2$, 1.5% $Er:LaAlO_3/ZrO_2$, 1% $Nd:YAG/HfO_2$, and 3% $Nd:YAG/HfO_2$. [147]

Figure 14. (a) A schematic illustration of the multianvil furnace apparatus used for the ultra-high pressure crystallization of glass; (b) Optical transmittance spectra of the $Ca_3Al_2Si_3O_{12}$ ceramic samples annealed at different temperatures; (c) Transparent $Ca_3Cr_2Si_3O_{12}$ (green), $Mg_3Al_2Si_3O_{12}$ (colorless), and $Mg_3Cr_2Si_3O_{12}$ (purple) garnet nanoceramics fabricated at 1400°C and 15 GPa applied pressure using the multianvil furnace; (d) Photographs and SEM images of $Ca_3Al_2Si_3O_{12}$ transparent ceramics samples obtained by annealing at 1300–1500°C at 15 GPa applied pressure. [148]

Author biographies

Iva Milisavljevic

Iva Milisavljevic is a PhD student in Ceramic Engineering at Alfred University working in Dr. Yiquan Wu's research group. Her research interests include processing of transparent ceramics and epitaxial films for optical applications and the growth of single crystals of oxide materials using the solid-state single crystal growth approach.

Michael J. Pitcher

Dr Michael J. Pitcher studied inorganic solid state chemistry at the University of Oxford (D.Phil, 2011), before moving to the University of Liverpool where he specialised in the synthesis and characterisation of new functional oxide materials. In 2019 he was appointed as a CNRS researcher at CEMHTI (Orléans), with a Guest Fellowship award at LE STUDIUM Loire Valley Institute for

Advanced Studies. His current research interests lie in the discovery of materials with new compositions and structures by low temperature crystallisation techniques.

Jianqiang Li

Dr. Jianqiang Li is a professor at School of Materials Science and Engineering, University of Science and Technology Beijing since 2021. He received his PhD from Tsinghua University in 2004. From 2004 to 2006, he worked as a JSPS fellow at the Department of Materials, the University of Tokyo. Then he worked at the Institute of Process Engineering, Chinese Academy of Sciences from 2006-2021. His research interests mainly focus on transparent ceramics, high entropy glass/ceramics, phase change materials for heat storage, and solidification of oxide melts under microgravity.

Sébastien Chenu

Dr Sébastien Chenu received his PhD degree from the University of Rennes 1 (France) in 2009. From 2010 to 2014, he has worked as a temporary researcher in different laboratories (in France: ISCR - Rennes, CEMHTI - Orléans and ICMCB - Bordeaux), and in Canada (Zwanziger lab - Halifax). In 2014, he joined the University of Limoges as an associate professor at the IRCER laboratory. His current research interests are focused on transparent materials for optical applications: (i) development of transparent (glass-)ceramics via controlled crystallization of the parent glass, (ii) elaboration of transparent ceramics by powder sintering.

Mathieu Allix

Dr Mathieu Allix received his PhD degree from the University of Caen (France) in 2004. After three years at the University of Liverpool (U.K.), he joined the CNRS at the CEMHTI laboratory in Orléans (France) in 2007. His research interests include (i) crystallization mechanisms in oxide glasses with an application to the elaboration of transparent (glass-)ceramics and (ii) the synthesis and structural determination of new inorganic materials by electron microscopy and diffraction. He was laureate of the 2013 CNRS bronze Medal.

Yiquan Wu

Dr. Yiquan Wu is a Professor of ceramics and materials science at the Kazuo Inamori School of Engineering at the New York State College of Ceramics at Alfred University. He received PhD from Imperial College London, England. His current research focuses on transparent materials for optical and photonic applications, but his research experience also includes the synthesis and characterization of nanostructured materials for energy and biomedical applications at Duke University and University of Rochester.